Liquid-Liquid Flow at Nanoscale: Slip and Hydrodynamic Boundary Conditions

Lolita Hilaire, Bertrand Siboulet, Sophie Charton, Jean-François Dufrêche

Liquid-liquid flow at nanoscale: slip and hydrodynamic boundary conditions

Lolita Hilaire,[†,‡] Bertrand Siboulet,[¶,‡] Sophie Charton,[*,†,‡] and Jean-François Dufrêche[*,¶,‡]

†*CEA, DES, ISEC, DMRC, Univ Montpellier, Marcoule, France.*

‡*Centre CEA Marcoule, BP 17171 30207 Bagnols-sur-Cèze Cedex, France*

¶*ICSM, CEA, CNRS, Univ Montpellier, Marcoule, France.*

E-mail: sophie.charton@cea.fr; jean-francois.dufreche@icsm.fr

Abstract

Non-Equilibrium Molecular Dynamics (NEMD) simulations have been performed to describe the flow of a fluid nanolayer confined by another fluid. The results show that the behaviour of liquids can still be described by the Navier-Stokes equation at the nanoscale, *i.e.* when only few molecular layers are involved. NEMD furthermore gives additional knowledge on flow. Indeed, while a very small slip is evidenced for a solid-liquid interfaces, as *e.g.* in lubrication, the slip lengths are significantly larger at the liquid-liquid interface, as encountered *e.g.* in droplets coalescence. The slip lengths of the two fluids are linked. The increase in hydrodynamic slip for liquid-liquid interfaces is attributed to the enhancement of fluid diffusion, which reduces friction.

Introduction

Behaviour of fluids confined in nanochannels are of great interest in many fields from theoretical and industrial point of view. For instance, developments in nanoscience led to the

emergence of nanofluidic devices, and it is important to understand the physics of fluids at that scale. Navier-Stokes equations are commonly used to describe flows at macro and meso scale, and for a long-time the no-slip condition was adopted. However, in the past decades, many results from experiments and simulations have highlighted the presence of slip at the solid-liquid interface, especially at nanoscale.[1] In the vicinity of the wall, the fluid is layered due to its molecular structure.[2] The interaction with a wall can modify the local order in the liquid near the solid and have an effect on flow and slip.[3] When a fluid is confined in a nano-pore, the flow properties differ from those at macro and micro scale because the interaction between the fluid and the wall plays an important role.[4] As a results, many studies were carried to assess the relevance of Navier-Stokes equations to describe the hydrodynamics of a fluid confined in a nanochannel. One of the best tool used to describe confined fluid is computer simulation.[5] In particular, non equilibrium molecular dynamics (NEMD) simulations have been widely used for the simulation of viscous homogeneous fluid flows.[6] With that technique, it has been shown the Navier-Stokes equations were accurate if the width of the pore is much larger than 10 times the molecular size.[7,8] The behaviour of water in a confined domain of a few nanometers was shown to be well predicted by the Navier-Stokes equation using the bulk properties of the fluid.[9,10] The flow and transport in nanofluidics can be influenced by many parameters which aroused great interest in the scientific community.[11] In particular, many studies focused on the phenomenon of slip at solid-liquid interface.

The hydrodynamic boundary conditions can also be studied by molecular dynamics simulations. Slippage may occur at the interface and slip lengths can be calculated from non equilibrium[12–14] and equilibrium[15,16] molecular dynamics simulations. NEMD simulations may have limits when it comes to quantifying the slip length of a liquid on a channel when its value becomes large.[17] Although giant slip values have been obtained and well modelled by MD with the use of hydrophobic ball bearings.[18] In any case it is undeniable that the existence of slip has been well highlighted. The slip length, however, depends on many pa-

rameters such as the fluid temperature,[19,20] the surface roughness and its polarity.[21] Slip is highly influenced by charged surfaces which alter the structure of the electrical double layer contribute to friction.[22–24]

Surprisingly there are very few similar molecular studies of hydrodynammic boundary conditions at liquid-liquid interfaces. Yet many industrial processes such as nuclear fuel treatment, recycling and separating chemistry involve the mixing or demixing of two liquid phases. Understanding how liquid-liquid interfaces respond to stress is of great interest for the development and optimisation of these processes. Phenomena like film thinning,[25,26] droplet coalescence[27,28] or mass transfer[29] are directly controlled by the behaviour and the properties of the liquid interface. However, the understanding of the liquid interface dynamics remains a major challenge because it lacks description at the nano-scale. At the macro-scale, the classical boundary conditions is that there is equality of the tangential velocity at the liquid-liquid interface except from some systems of polymers where a slip can be considered.[30,31] The recognition and consideration of slip at the solid-liquid interface has led to great improvement in the field of nanofluidics. Similarly, a better understanding of the slip at liquid-liquid interfaces could lead significant improvements in the aforementioned processes. Several works highlighted the presence of slip at a fluid-fluid Lennard-Jones interface by MD simulations.[32–34] However, a full explanation of the slip in fluids not composed of chain-like molecules is not given. The slip is an apparent jump in velocity and can be modelled effectively via a Navier Slip Condition.[35,36] This theory is supported by the apparent relation between the slip length and the viscosity of the fluid. Recently, the behaviour of a laminar two-phase flow in quartz nanopores was investigated.[37] The authors pointed out that liquid-liquid slip has a strong influence on the non wetting-phase flow. By taking into account the liquid-liquid slip in the theoretical hydrodynamics model, they improved the description and understanding of the mechanisms occurring in confined multi-phase flow.[37]

In the present work, we used NEMD simulations and hydrodynamics theory to study the flow of confined liquids and the slip at the interfaces. The liquids are confined either in a solid channel or between two other immiscible liquid layers. We report molecular simulations of water flow in frozen heptane nanochannels and heptane flow in frozen water nanochannels. We also carried MD simulations in the case of a two phase system composed of liquid water and liquid heptane separated by a planar interface. Due to periodic boundary conditions, each liquid is confined between two layers of the other one. In this case, the two liquids are mobile and undergoing flow in opposite directions. We calculated the viscosity of bulk heptane and bulk water using the Green-Kubo method. We then use NEMD simulations to obtain the velocity profiles in the different confined liquids modelled. To make sure the velocity fitting is not arbitrary,[38–40] we have taken the Gibbs convention for the interface position for both water and heptane. These profiles were compared to the prediction of a continuous hydrodynamics model resulting from the resolution of Navier-Stokes equation with slip boundary conditions. The aim of this is to assess the relevance of a continuous hydrodynamic description of confined liquids at the nano-scale and to study the influence of interface mobility on slip.

Methods and models

Molecular Dynamics

In the present simulations, we study the flow in confined liquid heptane and in confined liquid water. The models used for MD simulations are rigid SPC/E for water[41,42] and OPLS for n-heptane.[43] Particles interact through Lennard-Jones (LJ) and Coulomb potentials. A cut-off of 12 Å is used for LJ interactions and a PPPM solver is used to compute long-range Coulomb interactions.[44] The SHAKE[45] algorithm is used in the integration of the equation of motion for the rigid SPC/E model. The study is divided in two parts. In the first part, one component is liquid and the other is made rigid by the simulation parameters. This

is equivalent to the simulation of a liquid flow in a nanochannel. In the second part, both components are liquid and are subjected to flows in opposite directions. The first part was carried out for comparison with the solid/liquid case in order to understand the mechanisms underlying the liquid/liquid interfaces.

In the solid-liquid case, we model liquid water confined between two frozen heptane surfaces, and liquid heptane confined between two frozen water surfaces. The use of the term frozen refers here to the fact that molecules are kept rigid and immobile during the simulation. In each case, we model channels of 8 and 12 nm width. The dimensions of the computational box were chosen so as to obtain at equilibrium, taking into account the role of the surface tension, plane interfaces between the two liquids. Indeed, according to the aspect ratio of the box, the interface obtained will be spherical, cylindrical or planar.[46] The dimensions of the box in the x and y directions chosen are 7 and 3.6 nm respectively.

In the liquid-liquid case, both water and heptane are liquid and separated by a planar interface. No constraints were applied on the mobility of the interface, but the surface tension between heptane and water is large enough to show small fluctuations. Due to periodic boundary conditions, a layer of heptane is confined between two layers of water and reciprocally. We study two different configurations: (1) a system composed of an 8 nm heptane layer and an 8 nm water layer, and (2) a system composed of a 12 nm heptane layer and a 12 nm water layer. Details of the systems dimensions are provided in Table 1.

Table 1: Dimensions of the modelled systems.

Num	x	y	z	Heptane layer	Water layer
1	7 nm	3.6 nm	16 nm	8 nm	8 nm
2	7 nm	3.6 nm	24 nm	12 nm	12 nm

After each system is constructed, a minimisation is performed. The systems are then equilibrated in the NPT ensemble at 298 K and 1 atm for 2 ns. All MD simulations are

carried out with LAMMPS.[47] Temperature in this configuration has to be kept constant otherwise the box will heat up. It is maintained constant with a Nose-Hoover[48] thermostat. In some cases, the use of thermostat in confined fluids can lead to unphysical simulation artefacts.[49,50] Several thermostat has been tested in the simulations and no artefacts were observed. The thermostat was not decoupled in any spatial direction due to possible issues one may encounter while using rigid molecules.[51]

To study the hydrodynamics in heptane and water layers, a Poiseuille flow was induced by applying constant external forces on each atoms of the liquids along the x-axis. In the studied liquid-liquid configuration, forces and flows in each liquid were in opposite directions. Hence, to ensure the stability of the simulation, the resulting component of the forces must be zero. In both solid-liquid and liquid-liquid configurations, we simulated flows for four different external forces to make sure that simulations are performed in the linear response regime. The results for the weakest force computed were very noisy, sometimes resulting in "v"-shaped profile and thus not relevant. We have hence removed these results from the calculations of average slip lengths. We present results for only one of the forces, F, for greater clarity. F represents the total force applied to the considered liquid layer and is given by:

$$F = N_C f_C + N_H f_H \quad \text{or} \quad F = N_{O_w} f_{O_w} + N_{H_w} f_{H_w}, \tag{1}$$

where f_{C} is the force applied on the carbon and f_{H} the one applied on the hydrogen atom of the heptane molecule, and $f_{\mathrm{O_w}}$ and $f_{\mathrm{H_w}}$ the forces applied on the oxygen and hydrogen atom of the water molecule respectively. N_C, N_H, N_{O_w} ,N_{H_w} are the number of each atoms in the considered liquid. The ratios of the force applied on the carbon f_{C} and hydrogen f_{H} atoms $f_{\mathrm{O_w}}/f_{\mathrm{H_w}}$ and $f_{\mathrm{C}}/f_{\mathrm{H}}$ are fixed by the ratio of the atomic masses so that all atoms have the same acceleration. This method is applied to avoid disturbing the rotation of the molecules. Table 2 reports the four total forces exerted on the heptane layers to ensure flows in both widths considered along with the forces applied on the carbon and hydrogen atoms of the

heptane molecule. Table 3 reports the four total forces exerted on the water to ensure flows in both channel widths considered along with applied on the oxygen and hydrogen atoms of the water molecule.

Table 2: Applied forces on the heptane layer and corresponding forces applied on carbon f_{C} and hydrogen f_{H} atoms of the heptane molecule for the different systems constructed.

Total force (kcal·(mol·Å)$^{-1}$)	Layer	f_{C} (kcal·(mol·Å)$^{-1}$)	f_{H} (kcal·(mol·Å)$^{-1}$)
$F_1 = -0.379239$	8 nm	-5.5×10^{-5}	-4.61×10^{-6}
$F_1 = -0.379239$	12 nm	-3.66×10^{-5}	-3.07×10^{-6}
$F_2 = -0.758479$	8 nm	-1.1×10^{-4}	-9.21×10^{-6}
$F_2 = -0.758479$	12 nm	-7.3×10^{-5}	-6.14×10^{-6}
$F_3 = -1.8962$	8 nm	-2.75×10^{-4}	-2.3×10^{-5}
$F_3 = -1.8962$	12 nm	-1.8×10^{-4}	-1.53×10^{-5}
$F_4 = -2.8443$	8 nm	-4.12×10^{-4}	-3.5×10^{-5}
$F_4 = -2.8443$	12 nm	-2.7×10^{-4}	-2.3×10^{-5}

Table 3: Applied forces on the water layer and corresponding forces applied on the oxygen $f_{\mathrm{O_w}}$ and hydrogen $f_{\mathrm{H_w}}$ atoms of the water molecule for the different systems constructed.

Total force (kcal·(mol·Å)$^{-1}$)	Layer	$f_{\mathrm{O_w}}$ (kcal·(mol·Å)$^{-1}$)	$f_{\mathrm{H_w}}$ (kcal·(mol·Å)$^{-1}$)
$F_1 = 0.379239$	8 nm	5.0×10^{-5}	3.15×10^{-6}
$F_1 = 0.379239$	12 nm	3.3×10^{-5}	2.1×10^{-6}
$F_2 = 0.758479$	8 nm	1,0×10^{-4}	6.3×10^{-6}
$F_2 = 0.758479$	12 nm	6.64×10^{-5}	4.2×10^{-6}
$F_3 = 1.8962$	8 nm	2.5×10^{-4}	1.6×10^{-5}
$F_3 = 1.8962$	12 nm	1.66×10^{-4}	1.05×10^{-5}
$F_4 = 2.8443$	8 nm	3.75×10^{-4}	2.36×10^{-5}
$F_4 = 2.8443$	12 nm	2.49×10^{-4}	1.57×10^{-5}

In the cases presented in this paper. In this paper, we present the results for $F = \pm 2.8443$ kcal·(mol·Å)$^{-1}$, depending on whether the force is applied according to $+x$ or $-x$. This value corresponds to a linear response regime, as was verified by simulating four different external forces in both solid-liquid and liquid-liquid configurations. Results are available as Appendix. This includes velocity profiles normalized by the applied force, so as to establish the response linearity. In simulations, atoms trajectories are collected every 0.5 ps for 10 ns. Velocities and densities of the particles in the x direction are sampled each femtosecond in bins of 0.2

Å over the z axis, and averaged over the total simulation.

Green-Kubo calculations

MD profiles have been fitted to profiles from continuous hydrodynamics theory so as to deduce the slip lengths. Since these models include the viscosity of the fluids involved as unknown parameters, we calculated the viscosity at 298 K and 1 atm of SPC/E water and OPLS n-heptane using the Green-Kubo formula.[52–54] The Green-Kubo formula links the bulk viscosity to the auto-correlation function of the diagonal and cross components of the stress tensor $P_{\alpha\beta}$:

$$\eta_{\mathrm{GK}} = \frac{V}{k_B T} \int_0^\infty \langle P_{\alpha\beta}(0) P_{\alpha\beta}(t) \rangle dt. \tag{2}$$

SPC/E Water

For the Green-Kubo calculation of the viscosity of SPC/E water we use a system of 6736 water molecules. We collect the 5 components of the stress tensor (P_{xy},P_{xz},P_{yz},1/2(P_{xx} − Pyy),1/2($P_{yy} - P_{zz}$)) every femtosecond. The auto-correlation function (ACF) is averaged over all the components of the stress tensor. The viscosity is then obtained from the integral of the ACF over 5 ps. The ACF and the integral are given in Figure 1. We obtain a viscosity of $\eta_{\mathrm{SPC/E}} = 0.787$ mPa·s which is consistent with the literature values for the same model.[55,56]

OPLS n-Heptane

For the calculation of the viscosity of OPLS n-heptane we use a system of 826 heptane molecules. As before we collect the 5 components of the stress tensor every femtosecond and average the ACF over all the components. The viscosity is then obtained from the integral of the ACF over 5 ps. The ACF and the integral are given in Figure 2. We obtain

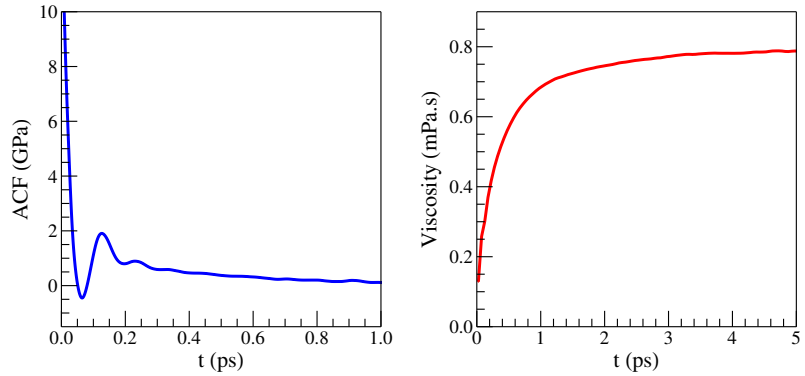

Figure 1: Auto-correlation function (left) and integral over 5 ps (right) for SPC/E water.

a viscosity of $\eta_{\mathrm{OPLS}} = 0.387$ mPa·s. Viscosities derived from Green-Kubo are available for some n-alkanes[57,58] but that of n-heptane is not given specifically. The value we calculated is, however, consistent with the viscosity obtained for mixtures with high n-heptane mole fractions.[59,60]

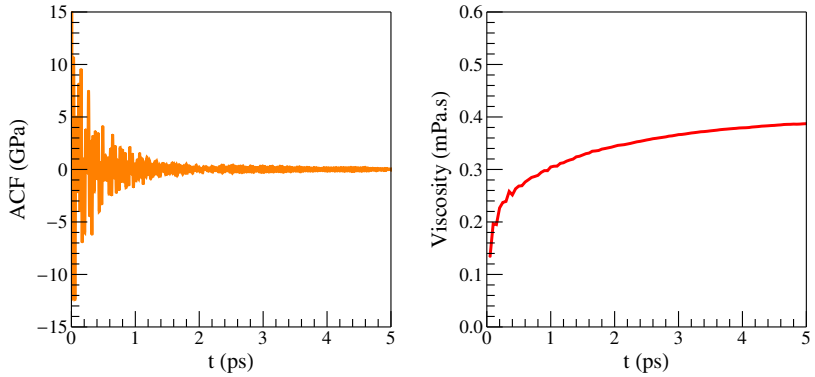

Figure 2: Auto-correlation function (left) and integral over 5 ps (right) for OPLS n-heptane.

Hydrodynamics treatment

In continuous hydrodynamics models, flows at low Reynolds number are described by Stokes equation which states:

$$\eta \Delta \mathbf{v} - \nabla P + \mathbf{f_v} = \mathbf{0}, \tag{3}$$

where η is the viscosity of the fluid, $\mathbf{v}$ is the velocity field, P the pressure, and $\mathbf{f_v}$ the external force density exerted on the fluid. The equations have been solved, assuming fluid

incompressibility, for the two configurations studied. The detailed steps of the calculations are available as SI.

In the case of a confined liquid (Fig. 3), the flow is described by Eq.(16). Regarding the boundary conditions, we consider that slip is prevailing. If there is a slip in $z = L/2$, considering Navier's condition, L being the channel width, the velocity profile is parabolic:

$$v = -\frac{f_v}{2\eta}\left(z^2 + Lb - \frac{L^2}{4}\right). \tag{4}$$

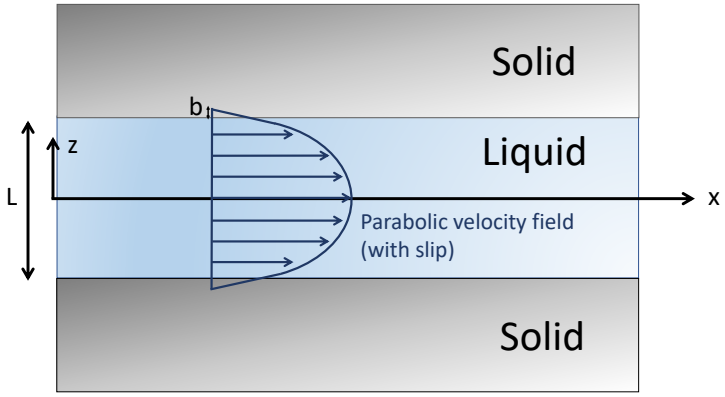

Figure 3: Poiseuille flow in a confined solid with slip boundary conditions.

The case of two liquids in PBC is shown in Fig. 4. For a stationary state, the total linear momentum is constant so that:

$$\int_{L_1} f_1 \mathrm{d}z - \int_{L_2} f_2 \mathrm{d}z = 0, \tag{5}$$

with f_1 and f_2 the forces applied on liquid 1 and liquid 2 respectively. Both fluids follow the Stokes equation. At the two fluid interfaces, slip boundary condition (SBC) applies, with two distinct values b_1 and b_2 for the slip lengths. The consistency of the calculation (see

Appendix for details) requires that a relation exists between the two slip lenghts:

$$\frac{b_1}{\eta_1} = \frac{b_2}{\eta_2}. \tag{6}$$

The ratio of the slip length to the viscosity is in fact the interaction force between the fluids and is therefore the same due to Newton's third law. We introduce the notation $\frac{b_1}{\eta_1} = \frac{b_2}{\eta_2} = \frac{b}{\eta}$ in the following. The final expressions of the velocities are (see Appendix for details):

$$\begin{cases} v_1 &= \frac{f_1}{2\eta_1}\left(\left(\frac{L_1}{2}\right)^2 - z^2\right) + \bar{v} + \left(1 + \frac{L_2\rho_2 - L_1\rho_1}{\rho_1 L_1 + \rho_2 L_2}\right)\frac{v_g}{2} \\ v_2 &= -\frac{f_2}{2\eta_2}\left(\left(\frac{L_2}{2}\right)^2 - z^2\right) + \bar{v} - \left(1 + \frac{L_1\rho_1 - L_2\rho_2}{\rho_1 L_1 + \rho_2 L_2}\right)\frac{v_g}{2} \end{cases} \tag{7}$$

with:

$$\bar{v} = \left(\frac{\rho_2 L_2^2}{12\eta_2} - \frac{\rho_1 L_1^2}{12\eta_1}\right)\frac{fL}{\rho_1 L_1 + \rho_2 L_2}. \tag{8}$$

The slip velocity v_g at the interfaces reads:

$$v_g = v_1 - v_2 = \frac{b}{2\eta} fL. \tag{9}$$

We thus have two opposite Poiseuille flows and constant velocity, which depends on the reference frame (see Fig. 4).

Results and Discussion

Liquid flow in a nanochannel

Let us now compare the hydrodynamic model to MD simulations. For a liquid confined in a rigid channel, hydrodynamics predicts a parabolic velocity profile described by Eq.(26). We use NEMD to simulate the flow of liquid heptane in frozen water channels of 8 and 12 nm widths, and reciprocally, the flow of liquid water in frozen heptane channels of 8 and 12 nm widths. For each system and channel widths we considered, four simulations are carried out

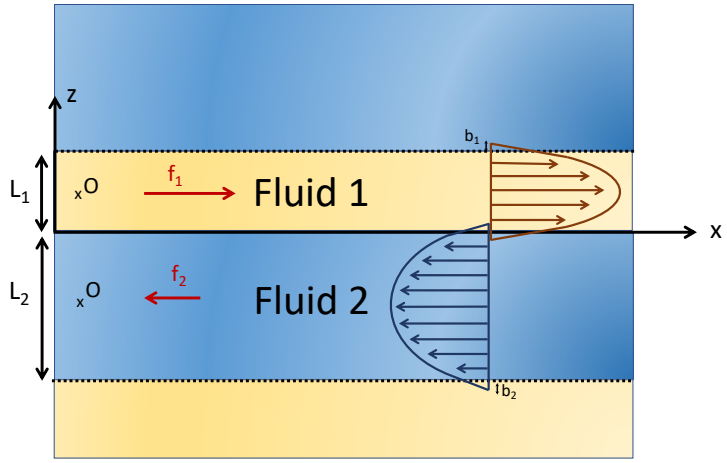

Figure 4: Opposite Poiseuille flows within fluids in slab geometry.

with various applied forces. In this section, we present the results for only one of the forces computed and only for the 8 nm channel. The results for all computed forces in both channel widths are available as SI for the two systems considered.

Fig. 5 reports the density profiles and the velocity profiles obtained for a heptane flow in a 8 nm frozen water channel. The total force applied on the heptane layer is $F = -2.8443$ kcal·(mol·Å)$^{-1}$. A snapshot of the simulation is also presented in Fig. 5 with some heptane molecules coloured in red in order to visualise the Poiseuille flow. The movie of this simulation is available as SI. Velocity profiles are fitted with eq. 26 to deduce the slip length of heptane on rigid water $b^{\mathrm{s}}_{\mathrm{h/w}}$. To increase the accuracy, we use a function that calculates the difference between the MD profile and the one predicted by eq. 26. The parameter $b^{\mathrm{s}}_{\mathrm{h/w}}$ is adjusted so that the function is minimised. We obtain a value of $b^{\mathrm{s}}_{\mathrm{h/w}} = 2.2$ Å for $F = -2.8443$ kcal·(mol·Å)$^{-1}$ in the 8 nm channel. The slip length values obtained for different channel widths and forces F_2 to F_4 are given as Appendix along with the corresponding density and velocity profiles. Results for F_1 were too noisy to be relevant.

Fig. 6 represents the density and velocity profiles obtained for a water flow in a 8 nm frozen

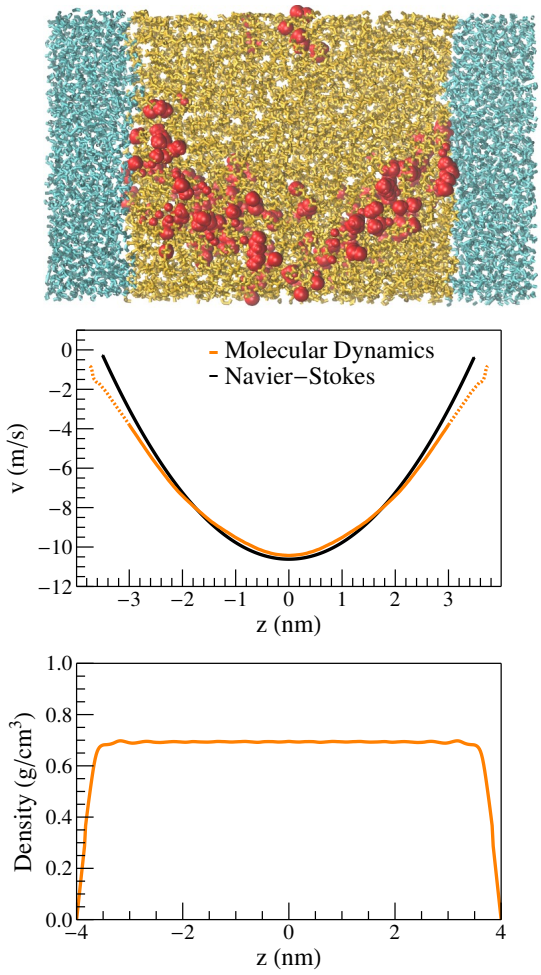

Figure 5: Snapshot of heptane flow (in orange and red) in a frozen water channel (in cyan). Velocity and density profiles obtained from NEMD simulations for heptane (in orange) and profile predicted by Navier-Stokes equations (in black) for flow in a channel of 8 nm-width for $F = -2.8443$ kcal·(mol·Å)$^{-1}$.

heptane channel. The total force applied on the water layer is $F = 2.8443$ kcal·(mol·Å)$^{-1}$. A snapshot of the simulation on which some water molecules have been coloured in green in order to follow their motion is also presented in Fig. 6. The movie of this simulation is available as SI. A Poiseuille flow is clearly observed. In this case also, MD profiles are fitted with eq. 26. The slip length of water on frozen heptane $b^{\mathrm{s}}_{\mathrm{w/h}}$ is deduced from the minimisation of the deviation between the MD profile and the profile predicted by the continuous model. The value obtained is $b^{\mathrm{s}}_{\mathrm{w/h}} = 2.4$ Å in the 8 nm channel for a total applied force $F = 2.8443$ kcal·(mol·Å)$^{-1}$. Like in the heptane case, other forces belonging to the linear

regime are computed for both the 8 nm and the 12 nm channel. The slip lengths obtained for all the forces computed in both channels are given as SI.

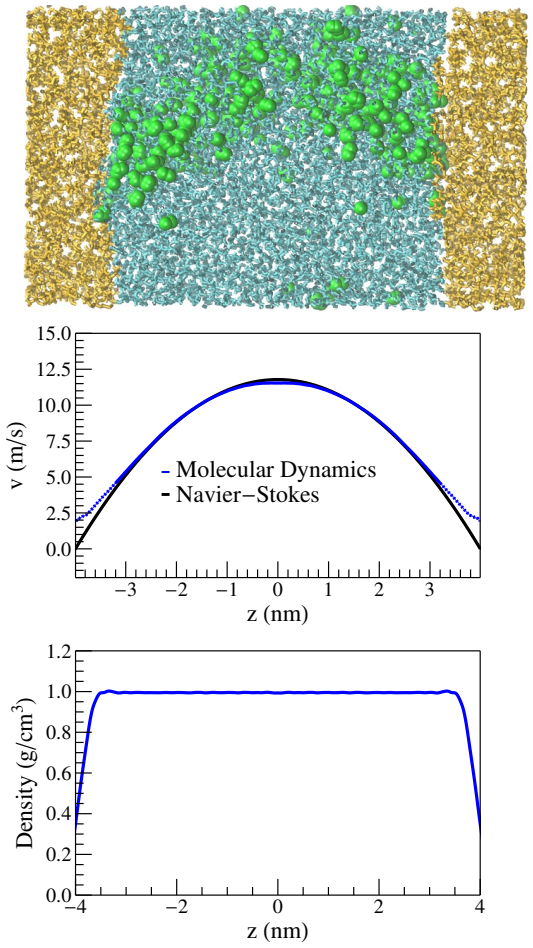

Figure 6: Snapshot of water flow (in cyan and green) in a frozen heptane channel (in orange). Velocity and density profiles obtained from NEMD simulation for water (in blue) and profiles predicted by Navier-Stokes equations (in black) for a flow in a channel of 8 nm width for $F = 2.8443$ kcal·(mol·Å)$^{-1}$.

For both heptane and water flows in a solid nanochannel, the velocity profiles obtained are parabolic and correspond to the predicted curvature for all the forces computed. The deviation of the hydrodynamic prediction from the MD simulation results is very small, as can be seen by adding all the curves (see Figure 9). The viscosity of the liquid in the channel is hence equal to that of the bulk within calculations uncertainties, and its behaviour

can be predicted by the Stokes equation with slip boundary conditions. Removing the results form the weakest force, the average slip length of liquid heptane on frozen water is $b^{s}_{h/w} = 1.36 \pm 0.05$ Å , and the average slip length of liquid water on frozen heptane $b^{s}_{w/h} = 1.75 \pm 0.04$ Å. For both water and heptane, the slip at the solid-liquid interface is very small. Slip at solid-liquid interface has been known to decrease with charge density.[23] It is also influenced by temperature and can increase drastically in the case of super-cooled fluids.[19] This result obtained for a solid/liquid interface shows that the rigidity of the "frozen" surface is likely to immobilize the molecules and reduce sliding, as we will now see by comparing with the case where the two parts are fluid.

Two phase flow with liquid-liquid planar interface

In the liquid-liquid configuration, both water and heptane are liquid and in a periodic slab configuration with planar liquid-liquid interfaces. The aim is here to assess the relevance of continuous hydrodynamics models to describe the behaviour a liquid film trapped between two layers of a non-miscible liquid. We also investigate the effects that switching from a solid to a liquid interface may have on the slip. NEMD simulations are used to apply forces in opposite directions on heptane and water. The forces have to compensate each other to ensure stability of the simulation. Details of the simulations are provided in the Molecular Dynamics section. Two configurations are studied : (1) a 8 nm heptane layer with a 8 nm water layer, and (2) a 12 nm heptane layer with a 12 nm water layer. Two movies are available as SI, one for each configuration. To visualise the flows, some water molecules have been coloured in green and some heptane molecules in red. In both cases, Poiseuille flows in opposite directions can be observed.

In this section we only present the velocity and density profiles obtained in the 8 nm/8 nm configuration for a total force of $F = 2.8443$ kcal·(mol·Å)$^{-1}$ applied on water and a total force of $F = -2.8443$ kcal·(·Å)$^{-1}$ applied on heptane. For the sake of simplicity, and since

in each case the forces applied on the liquids compensate each other, F will refer as the absolute value of the force applied on the corresponding liquid. Fig. 7 represents the aforementioned profiles along with a snapshot of the simulation in which some heptane molecules are coloured in red and some water molecules are coloured in green. This allows to visualise the Poiseuille flows from the trajectory and clarify the comparison with the velocity profiles. For the two studied configurations, four external force fields were computed. All velocity and density profiles we obtained are available as SI.

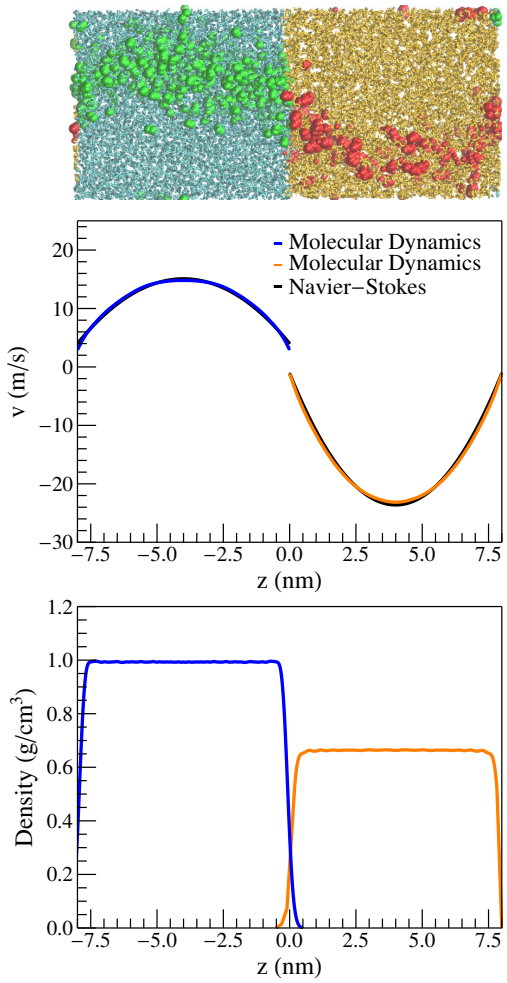

Figure 7: Snapshot of Poiseuille flows in heptane (in orange and red) and water (in cyan and green) for a total force $F = \pm 2.8443$ kcal·(mol·Å)$^{-1}$ applied on each liquid. Velocity and density profiles obtained from NEMD simulations for heptane (in orange) and for water (in blue) and profiles predicted by Navier-Stokes equations (in black) for a system with 8 nm layers.

In all the cases we considered, the heptane and water profiles are parabolic and in opposite directions, the curvatures obtained follow the predictions of the Poiseuille law. However, for the continuous model to be consistent, the following relation must be satisfied:

$$r_{\mathrm{h}} = \frac{b^{\mathrm{L}}_{\mathrm{h/w}}}{\eta_{\mathrm{h}}} = \frac{b^{\mathrm{L}}_{\mathrm{w/h}}}{\eta_{\mathrm{w}}} = r_{\mathrm{w}}. \tag{10}$$

The velocity profiles obtained from molecular dynamics simulations have been fitted from the ones obtained by continuous hydrodynamics (Eq. (58)). In particular, slip lengths of water on liquid heptane $b^{\mathrm{L}}_{\mathrm{w/h}}$ and of heptane on liquid water $b^{\mathrm{L}}_{\mathrm{h/w}}$ are fitted so that deviation between the profiles resulting from Eq. 58 and the MD profiles is minimized. The ratio $r_{\mathrm{w}}/r_{\mathrm{h}}$ is then calculated. If this ratio is close to 1, it means that the condition given by Eq (10) is accurate. Table (4) sums up all the slip lengths $b^{\mathrm{L}}_{\mathrm{w/h}}$ and $b^{\mathrm{L}}_{\mathrm{h/w}}$ obtained in each configuration for all the forces computed, and the corresponding ratios $r_{\mathrm{w}}/r_{\mathrm{h}}$. The forces that were not introduced in this paper are referred to as fractions of the force F.

Table 4: Slip lengths of water on liquid heptane $b^{\mathrm{l}}_{\mathrm{w/h}}$ and of heptane on liquid water $b^{\mathrm{l}}_{\mathrm{w/h}}$ and corresponding ratios $r_{\mathrm{w}}/r_{\mathrm{h}}$ obtained in the two configurations studied for all the computed forces.

Layers	8 nm			
Force	F	$2/3F$	$4/15F$	Average
$b^{\mathrm{l}}_{\mathrm{w/h}}$ (nm)	1.1	1.05	1.01	1.05 ± 0.05
$b^{\mathrm{l}}_{\mathrm{h/w}}$ (nm)	0.45	0.52	0.45	0.47 ± 0.05
$r_{\mathrm{w}}/r_{\mathrm{h}}$	1.2	0.99	1.1	1.1 ± 0.1
Layers	12 nm			
Force	F	$2/3F$	$4/15F$	Average
$b^{\mathrm{l}}_{\mathrm{w/h}}$ (nm)	1.05	1.12	1.02	1.06 ± 0.06
$b^{\mathrm{l}}_{\mathrm{h/w}}$ (nm)	0.53	0.44	0.44	0.47 ± 0.06
$r_{\mathrm{w}}/r_{\mathrm{h}}$	0.97	1.25	1.14	1.12 ± 0.17

The size of the channel has no influence on the value of the slip lengths, and the response of the system is linear in the considered range of force. Results obtained for the lowest

force $2/15F$ were not taken into account in the average calculation because the corresponding velocity profiles are too noisy. The average slip length of water on liquid heptane is $b^{\mathrm{L}}_{\mathrm{w/h}} = 1.05 \pm 0.06$ nm which is 5 to 6 times higher than that of water on frozen heptane. Likewise, the average slip length of heptane on liquid water is $b^{\mathrm{L}}_{\mathrm{h/w}} = 0.47 \pm 0.06$ nm which is 3 times higher than that of heptane on frozen water. The slip lengths increase significantly when switching from a solid-liquid configuration to a liquid-liquid one.

Knowing the respective viscosity and slip length of the two liquids, the ratio $r_{\mathrm{w}}/r_{\mathrm{h}}$ has been calculated to check the equality given by Eq.(10). With an average ratio $r_{\mathrm{w}}/r_{\mathrm{h}}$ of 1.11 $\pm$ 0.17, we can consider that the relation is well verified. This confirms that Stokes equation is relevant for liquid-liquid in PBC with forces applied in opposite directions. Globally, all the MD profiles can be satisfactorily reproduced for the two distances and for all forces.

Origin and consequences of slip

The relation between slip lengths can be understood from a simple microscopic analysis. The friction coefficient between the two fluids or between a fluid and a solid wall can be obtained from a Green-Kubo (GK) relation,[12,61] *e.g.* for water on heptane:

$$\lambda_{\mathrm{w}} = \frac{\eta_{\mathrm{w}}}{b^{S}_{\mathrm{w/h}}} = \frac{1}{Ak_BT}\int_0^{+\infty} \langle F_f(t).F_f(0)\rangle_{\mathrm{eq}} \mathrm{d}t, \tag{11}$$

where F_f is the force between the two phases and A is the area of the interface. Globally the application of such formula is delicate because, in the case of a confined fluid, the integral diverges.[62] This expression is not used here to calculate an explicit value of the friction coefficient but to propose a rough estimate:[13,21,24,63,64]

$$\int_0^{+\infty} \langle F_f(t).F_f(0)\rangle_{\mathrm{eq}} \mathrm{d}t \approx \langle F_f^2\rangle \tau, \tag{12}$$

where τ is the relaxation time given by the diffusion of fluid on a characteristic distance inducing interactions between molecules σ; thus for water $\tau_{\mathrm{w}} \approx \sigma_{\mathrm{w}}^2/D_w$ with D_{w} the water diffusion coefficient. The mean squared interaction force scales as $\langle F_f^2 \rangle = CN_{\mathrm{w}} \left(\frac{\epsilon_{\mathrm{w}}}{\frac{\sigma_h + \sigma_{\mathrm{w}}}{2}} \right)^2 = C\rho_{\mathrm{w}} A \sigma_{\mathrm{w}} \left(\frac{\epsilon_{\mathrm{w}}}{\sigma} \right)^2$ where $\sigma = (\sigma_{\mathrm{w}} + \sigma_{\mathrm{h}})/2$. N_{w} and ρ_{w} are respectively the number and the density of water molecules. C is a geometrical factor which increases with the roughness. ϵ_{w} represents the interaction energy of one water molecule with the heptane wall. The GK relation Eq.(11) leads to the following expression of the slip length of water on a rigid heptane wall:

$$b_{\mathrm{w/h}}^{\mathrm{S}} = \frac{\eta_{\mathrm{w}} D_{\mathrm{w}} k_B T \sigma^2}{C\rho_{\mathrm{w}} \epsilon_{\mathrm{w}}^2 \sigma_{\mathrm{w}}^3}. \tag{13}$$

Despite its simplicity, this approach gives the basic ingredients to understand the origin of slip[21,24] and a more systematic and accurate derivation leads to very similar results.[13,14] A symmetrical formula is obtained for the slip length of heptane on a rigid water wall. On average, if the box size is big enough, $\langle F_{\mathrm{w/h}}^2 \rangle = \langle F_{\mathrm{h/w}}^2 \rangle$ so that $\rho_{\mathrm{w}} \epsilon_{\mathrm{w}}^2 \sigma_{\mathrm{w}} = \rho_{\mathrm{h}} \epsilon_{\mathrm{h}}^2 \sigma_{\mathrm{h}}$ and we finally obtain:

$$\frac{b_{\mathrm{w/h}}^{\mathrm{S}}}{b_{\mathrm{h/w}}^{\mathrm{S}}} = \frac{\eta_{\mathrm{w}} D_{\mathrm{w}} \sigma_{\mathrm{h}}^2}{\eta_{\mathrm{h}} D_{\mathrm{h}} \sigma_{\mathrm{w}}^2}. \tag{14}$$

In this work, the diffusion coefficient of heptane[65] is $D_{\mathrm{h}} = 3.7 \times 10^{-9}$ m^2·s^{-1} and the diffusion coefficient of water[55] is $D_{\mathrm{w}} = 2.97 \times 10^{-9}$ m^2 ·s^{-1}. These are bulk values taken in order to propose an interpretation of the difference between the solid-liquid slip length and the liquid-liquid slip length by modeling the different effects. The ratio $\frac{D_{\mathrm{w}} \eta_{\mathrm{w}}}{D_{\mathrm{h}} \eta_{\mathrm{h}}}$ which corresponds to the ratio of the hydrodynamic diameters, is around 1.6. Therefore Eq.(14) is valid if $\sigma_{\mathrm{w}} \approx \sigma_{\mathrm{h}}$, which makes sense considering that we compare the sizes of rigid grouping in the molecule (CH_2 and O). Globally, the water slip length is larger than that of heptane simply because the hydrodynamic diameter of water is smaller than the one of heptane.

A similar analysis can be done in the case of the liquid/liquid interface. First, it should be noted that the GK formula automatically yields the link between the slip lengths of the

two liquids $\frac{b^{\mathrm{L}}_{\mathrm{h/w}}}{\eta_{\mathrm{h}}} = \frac{b^{\mathrm{L}}_{\mathrm{w/h}}}{\eta_{\mathrm{w}}}$. The deviation between slip lengths is related to the relative diffusion coefficient $D = D_{\mathrm{w}} + D_{\mathrm{h}}$. The characteristic length to consider is the average $\sigma = \frac{\sigma_{\mathrm{h}}+\sigma_{\mathrm{w}}}{2}$ and the relaxation time reads $\tau = \frac{\sigma^2}{D}$. Within these assumptions, the GK yields to the following expression of the slip length of water:

$$b^{\mathrm{L}}_{\mathrm{w/h}} \approx \frac{\eta_{\mathrm{w}} k_B T}{C\rho_{\mathrm{w}}\sigma_{\mathrm{w}}\left(\frac{\epsilon_{\mathrm{w}}}{\sigma}\right)^2 \frac{\sigma^2}{D}} = \frac{\eta_{\mathrm{w}} k_B T D}{C\rho_{\mathrm{w}}\sigma_{\mathrm{w}}\epsilon^2_{\mathrm{w}}} = \frac{D\sigma^2_{\mathrm{w}}}{D_{\mathrm{w}}\sigma^2} b^{\mathrm{S}}_{\mathrm{w/h}}. \tag{15}$$

The geometry being similar to the solid/liquid case, $\sigma_{\mathrm{w}} \approx \sigma_{\mathrm{h}} \approx \sigma$. Therefore an enhancement of slip is expected due to the diffusion term. Indeed, the friction coefficient λ_{w} is smaller because the relative diffusion accelerates the relaxation of the interaction force so that the slip length is higher. In our case, $D/D_{\mathrm{w}} \approx 2.2$ whereas the ratio of the slip lengths is $b^{\mathrm{L}}_{\mathrm{w/h}}/b^{\mathrm{S}}_{\mathrm{w/h}} \approx 4.4$. Thus, the fact that relative diffusion enhance diffusion, which reduces friction, explain a part of the enhancement of the slip lengths. In addition to the enhanced diffusion due to collective effects at the liquid/liquid interface, the relaxation of the interaction force is also higher because the self-diffusion of each liquid at the interface is itself increased compared to the situation where the wall is solid. The interface deformation possibilities in the liquid/liquid case are indeed higher, which allows the local diffusion coefficients of the two fluids to be increased. Thus it can be said that in a general way the increase in diffusion for the liquid-liquid interface is probably the main reason for the increase in slip compared to the case where the wall is solid.

Conclusions

We have shown that hydrodynamics models deriving from Stokes equation solved with slip boundary conditions are relevant to describe the flow of heptane and water in solid channels of 8 nm and 12 nm widths. Slip lengths are deduced from the comparison between the velocity profiles issued from the NEMD simulations and those predicted by continuous hydrodynamics equations. Their values range from 1 to 2 Å , the slip at the solid-liquid

interface is therefore very small but cannot be neglected.

We also modelled the flows in layers of heptane and water in periodic boundary conditions. In that case also, the behaviour of the liquids can be described by the continuous hydrodynamics model resulting from Stokes equation solved with slip boundary conditions. Slip lengths are deduced from the fitting of the velocity profiles issued from NEMD simulations with those predicted by the continuous hydrodynamics model. Slip lengths are greater for a liquid/liquid interface than for a similar solid/liquid interface. The slip length of heptane on water has an average value of 0.425 nm and the one of water on heptane is 1 nm. The slip enhancement is probably mainly due to a diffusion enhancement for liquid-liquid interfaces. The equality relating the respective slip length and viscosity of each liquids predicted by the continuous hydrodynamics model and by statistical mechanics is retrieved by MD simulations.

To sum up, we demonstrate that molecular simulations are relevant to describe flow in nanochannels as long as proper boundary conditions are taken into account. The prevailing boundary conditions at a fluid/fluid interface are very different from the ones at a solid/liquid interface. The relaxation of forces is faster because a fluid interface allows for faster diffusion and because the diffusion is effective on both fluids. The friction is thus lower and the slip greater.

Acknowledgement

The authors thank CEA for the *amont-aval* PhD grant of L. Hilaire and the SIACY project for its financial support. This work was also granted access to the HPC resources of [TGCC/CINES/IDRIS] under the allocation 2019-A0070911087 made by GENCI (Grand Equipement National de Calcul Intensif).

Supporting Information Available

- Movies of MD simulations for solid-liquid and liquid-liquid flows: water molecules are colored in blue and heptane molecules in yellow, some water molecules are marked in green and some heptane molecules in red to follow the Poiseuille flow

Appendix

Detailed hydrodynamics treatment

In the present study, the flow is at low Reynolds and is hence described by Stokes equation which states:

$$\eta \Delta \mathbf{v} - \nabla P + \mathbf{f_v} = \mathbf{0}, \tag{16}$$

where η is the viscosity of the fluid, $\mathbf{v}$ is the velocity field in the flow, P the pressure, and $\mathbf{f_v}$ the force per unit of volume exerted on the fluid. The Stokes equation contains four unknown parameters (v_x, v_y, v_z, P), yet Navier-Stokes only gives three equations. We assume incompressible flow, which gives the additional equation:

$$\mathrm{div}(\mathbf{v}) = 0 \tag{17}$$

The equations have to be resolved for the two configurations studied: solid-liquid and liquid-liquid.

Case of a confined fluid

In the case of a confined liquid, the flow is described by eq.16. Regarding the boundary conditions, we consider that there is a slip. Using the relation known as Navier's condition we have:

$$\frac{\mathrm{d}\mathbf{v}}{\mathrm{d}z} = -\frac{v}{b}, \tag{18}$$

where b is the slip length. The laminar flow of a viscous fluid in a pipe is described by Poiseuille's law which relates the viscosity of the fluid to the flow velocity.

In the case of a flow in the x direction we have $\mathbf{v} = v(x,z)\mathbf{e_x}$. Moreover, if we consider the fluid incompressible then $\mathrm{div}(\mathbf{v}) = \mathrm{d}\mathbf{v}/\mathrm{d}x = 0$, hence: $\mathbf{v} = v(z)\mathbf{e_x}$. The Stokes equation then becomes:

$$\eta\frac{\mathrm{d}^2 v}{\mathrm{d}z^2} - \frac{\mathrm{d}P}{\mathrm{d}x} + f_v = 0. \tag{19}$$

At the nanoscale, the force density is small. Given the impossibility of directly simulating pressure gradients in systems with PBC, NEMD generally replaces the $-\mathrm{d}P/\mathrm{d}x$ pressure gradient by a volume force f_v of the same intensity. This is what we do:

$$\eta\frac{\mathrm{d}^2}{\mathrm{d}z^2} = -f_v. \tag{20}$$

After integration we get:

$$v = \frac{-f_v}{2\eta}z^2 + Az + B. \tag{21}$$

It is necessary to determine the value of A and B. The symmetry of the system gives $A = 0$. B depends on the boundary conditions. If there is a slip, Navier's condition yields:

$$\frac{\mathrm{d}v}{\mathrm{d}z} = \frac{v}{b}, \tag{22}$$

so that:

$$-\frac{f_v}{\eta}z = -\frac{f_v}{2\eta b}z^2 + \frac{B}{b}. \tag{23}$$

The slip being in $z = L/2$, we obtain:

$$-\frac{f_v L}{2\eta} = -\frac{f_v L^2}{8\eta b} + \frac{B}{b}, \tag{24}$$

which yields:

$$B = -\frac{f_v L b}{2\eta} + \frac{f_v L^2}{8\eta} = \frac{f_v}{2\eta}\left(\frac{L^2}{4} - Lb\right). \tag{25}$$

The expression of the fluid velocity in a channel of width L has a parabolic form:

$$v = -\frac{f_v}{2\eta}\left(z^2 + Lb - \frac{L^2}{4}\right). \tag{26}$$

Case of two fluids with forces in opposite directions

The stability in NEMD simulations is guaranteed by the compensation of the forces applied on each liquid. Thus we have:

$$\int_{L_1} f_1 \mathrm{d}z - \int_{L_2} f_2 \mathrm{d}z = 0. \tag{27}$$

The flows follow Stokes' equation. The solution is:

$$\begin{cases} v_1 &= -\frac{f_1}{2\eta_1} z^2 + A_1 z + B_1 \\ v_2 &= \frac{f_2}{2\eta_2} z^2 + A_2 z + B_2 \end{cases} \tag{28}$$

We study the configuration with slip, hence the boundary conditions gives (if z is oriented from the interface to the fluid):

$$\frac{\delta v}{\delta z} = \frac{v}{b}, \tag{29}$$

where v is the velocity with respect to the interface and b the slip length of the fluid at the interface. Each fluid is different from the other and therefore has its own slip length b_1 and b_2. For the geometry we considered, we have at the middle-interface:

$$\frac{\delta v_1}{\delta z} = \frac{v_1 - v_2}{b_1} \quad \text{and} \quad -\frac{\delta v_2}{\delta z} = \frac{v_2 - v_1}{b_2}. \tag{30}$$

This gives for liquid 1:

$$-\frac{f_1}{\eta_1}z_1 + A_1 = -\frac{f_1}{2b_1\eta_1}z_1^2 + \frac{A_1}{b_1}z_1 + \frac{B_1}{b_1} - \frac{f_2}{2\eta_2 b_1}z_2^2 - \frac{A_2}{b_1}z_2 - \frac{B_2}{b_1}. \tag{31}$$

Thus, at the intermediate interface that is for $z_1 = -L_1/2$ and $z_2 = L_2/2$ we have:

$$\frac{f_1 L_1}{2\eta_1} + A_1 = -\frac{f_1 L_1^2}{8\eta_1 b_1} - \frac{A_1 L_1}{2b_1} + \frac{B_1}{b_1} - \frac{f_2 L_2^2}{8\eta_2 b_1} - \frac{A_2 L_2}{2b_1} - \frac{B_2}{b_1}. \tag{32}$$

The boundary conditions also give for liquid 2:

$$-\frac{f_2}{\eta_2}z_2 - A_2 = \frac{f_2}{2\eta_2 b_2}z_2^2 + \frac{A_2}{b_2}z_2 + \frac{B_2}{b_2} + \frac{f_1}{2\eta_1 b_2}z_1^2 - \frac{A_1}{b_2}z_1 - \frac{B_1}{b_2}, \tag{33}$$

which yields in $z_1 = -L_1/2$ and $z_2 = L_2/2$:

$$-\frac{f_2 L_2}{2\eta_2} - A_2 = \frac{f_2 L_2^2}{8\eta_2 b_2} + \frac{A_2 L_2}{2b_2} + \frac{B_2}{b_2} + \frac{f_1 L_1^2}{8\eta_1 b_2} + \frac{A_1 L_1}{2b_2} - \frac{B_1}{b_2}. \tag{34}$$

The slip boundary conditions can also be applied at the bottom (or upper) interface, and give:

$$-\frac{\delta v_1}{\delta z} = \frac{v_1 - v_2}{b_1} \quad \text{and} \quad \frac{\delta v_2}{\delta z} = \frac{v_2 - v_1}{b_2}. \tag{35}$$

Thus, for liquid 1:

$$\frac{f_1}{\eta_1}z_1 - A_1 = -\frac{f_1}{2b_1\eta_1}z_1^2 + \frac{A_1}{b_1}z_1 + \frac{B_1}{b_1} - \frac{f_2}{2\eta_2 b_1}z_2^2 - \frac{A_2}{b_1}z_2 - \frac{B_2}{b_1}. \tag{36}$$

We then have at the bottom (or upper) interface for $z_1 = L_1/2$ and $z_2 = -L_2/2$:

$$\frac{f_1 L_1}{2\eta_1} - A_1 = -\frac{f_1 L_1^2}{8\eta_1 b_1} + \frac{A_1 L_1}{2b_1} + \frac{B_1}{b_1} - \frac{f_2 L_2^2}{8\eta_2 b_1} + \frac{A_2 L_2}{2b_1} - \frac{B_2}{b_1}. \tag{37}$$

The same conditions yield for liquid 2:

$$\frac{f_2}{\eta_2}z_2 + A_2 = \frac{f_2}{2\eta_2 b_2}z_2^2 + \frac{A_2}{b_2}z_2 + \frac{B_2}{b_2} + \frac{f_1}{2\eta_1 b_2}z_1^2 - \frac{A_1}{b_2}z_1 - \frac{B_1}{b_2}. \tag{38}$$

So in $z_1 = L_1/2$ and $z_2 = -L_2/2$:

$$-\frac{f_2 L_2}{2\eta_2} + A_2 = \frac{f_2 L_2^2}{8\eta_2 b_2} - \frac{A_2 L_2}{2b_2} + \frac{B_2}{b_2} + \frac{f_1 L_1^2}{8\eta_1 b_2} - \frac{A_1 L_1}{2b_2} - \frac{B_1}{b_2}. \tag{39}$$

For the resolution, (32) − (37) yields:

$$-2A_1 = -\frac{A_1 L_1}{b_1} - \frac{A_2 L_2}{b_1}. \tag{40}$$

Also (39) − (34) yields:

$$2A_2 = -\frac{A_2 L_2}{b_2} - \frac{A_1 L_1}{b_2}. \tag{41}$$

We deduce $A_1 = A_2 = 0$. The next operation $b_1\times$ (37) $+b_2\times$ (39) yields:

$$\frac{b_1 f_1 L_1}{2\eta_1} - \frac{b_2 f_2 L_2}{2\eta_2} = 0. \tag{42}$$

Also for (32) and (34), the operation $b_1\times$ (32) + $b_2\times$ (34) yields:

$$\frac{b_1 f_1 L_1}{2\eta_1} - \frac{b_2 f_2 L_2}{2\eta_2} = 0. \tag{43}$$

The same condition is obtained. With slip, a stationary regime is obtained only if the condition given by (43) is verified. In NEMD simulations, forces applied on the liquids compensate each other to ensure stability: $f_1 L_1 = f_2 L_2$, we then have:

$$\frac{b_1}{\eta_1} = \frac{b_2}{\eta_2}. \tag{44}$$

We deduce that (32) and (34) are equivalent and:

$$\frac{f_1 L_1}{2\eta_1} = -\frac{f_1 L_1^2}{8\eta_1 b_1} - \frac{f_2 L_2^2}{8\eta_2 b_1} + \frac{B_1 - B_2}{b_1}. \tag{45}$$

With $f_1 L_1 = f_2 L_2 = fL$ and $b_1/\eta_1 = b_2/\eta_2 = b/\eta$, we then have:

$$B_1 - B_2 = \frac{bfL}{2\eta} + \frac{fLL_1}{8\eta_1} + \frac{fLL_2}{8\eta_2}. \tag{46}$$

Hence:

$$B_1 - B_2 = \left(\frac{b}{2\eta} + \frac{L_1}{8\eta_1} + \frac{L_2}{8\eta_2}\right) fL. \tag{47}$$

With $b = 0$, we obtain the non slip configuration. We obtain the same equation from eq. (37) or eq. (39). We introduce a velocity v_0:

$$B_1 - \frac{f_1 L_1^2}{8\eta_1} - \frac{bfL}{4\eta} = B_2 + \frac{f_2 L_2^2}{8\eta_2} + \frac{bfL}{4\eta} = v_0. \tag{48}$$

We can then write:

$$\left\{ \begin{array}{rcl} v_1 & = & \frac{f_1}{2\eta_1}\left(\left(\frac{L_1}{2}\right)^2 - z^2\right) + \frac{bfL}{4\eta} + v_0 \\ v_2 & = & -\frac{f_2}{2\eta_2}\left(\left(\frac{L_2}{2}\right)^2 - z^2\right) - \frac{bfL}{4\eta} + v_0 \end{array} \right. \tag{49}$$

In the case where the average velocity is zero we have:

$$\begin{array}{c} \int_{-L_1/2}^{L_1/2}\left(\frac{\rho_1 f_1}{2\eta_1}\left(\left(\frac{L_1}{2}\right)^2 - z^2\right) + \frac{b_1 f_1 L_1 \rho_1}{4\eta_1} + v_0\rho_1\right)\mathrm{d}z \\ + \int_{-L_2/2}^{L_2/2}\left(-\frac{\rho_2 f_2}{2\eta_2}\left(\left(\frac{L_2}{2}\right)^2 - z^2\right) - \frac{b_2 f_2 L_2 \rho_2}{4\eta_2} + v_0\rho_2\right)\mathrm{d}z = 0 \end{array} \tag{50}$$

Which gives:

$$\frac{f_1 L_1^3 \rho_1}{12\eta_1} + \frac{\rho_1 b_1 f_1 L_1^2}{4\eta_1} + v_0 L_1 \rho_1 - \frac{f_2 L_2^3 \rho_2}{12\eta_2} - \frac{\rho_2 b_2 f_2 L_2^2}{4\eta_2} + v_0 L_2 \rho_2 = 0. \tag{51}$$

Finally:

$$v_0 = \left(\frac{\rho_2 L_2^2}{12\eta_2} - \frac{\rho_1 L_1^2}{12\eta_1} - \frac{bL_1\rho_1}{4\eta} + \frac{bL_2\rho_2}{4\eta}\right)\frac{fL}{\rho_1 L_1 + \rho_2 L_2}. \tag{52}$$

We can then write v_1 and v_2 with:

$$\bar{v} = \left(\frac{L_2^2 \rho_2}{12\eta_2} - \frac{L_1^2 \rho_1}{12\eta_1} \right) \frac{fL}{\rho_1 L_1 + \rho_2 L_2}. \tag{53}$$

We then get:

$$\begin{cases} v_1 &= \frac{f_1}{2\eta_1} \left(\left(\frac{L_1}{2} \right)^2 - z^2 \right) + \bar{v} + \frac{bLf}{4\eta} \left(1 + \frac{L_2\rho_2 - L_1\rho_1}{\rho_1 L_1 + \rho_2 L_2} \right) \\ v_2 &= -\frac{f_2}{2\eta_2} \left(\left(\frac{L_2}{2} \right)^2 - z^2 \right) + \bar{v} - \frac{bLf}{4\eta} \left(1 + \frac{L_1\rho_1 - L_2\rho_2}{\rho_1 L_1 + \rho_2 L_2} \right). \end{cases} \tag{54}$$

Regarding the slip at the interfaces, we have:

$$v_1 - v_2 = \frac{f_1 L_1^2}{8\eta_1} + \frac{f_2 L_2^2}{8\eta_2} - \frac{f_1}{2\eta_1} z_1^2 - \frac{f_2}{2\eta_2} z_2^2 + \frac{bLf}{2\eta}. \tag{55}$$

Which gives at the middle-interface $z_1 = -L_1/2$ and $z_2 = L_2/2$:

$$v_1 - v_2 = \frac{bfL}{2\eta}. \tag{56}$$

We also find this expression at the bottom (or upper) interface in $z_1 = L_1/2$ and $z_2 = -L_2/2$.

We can interpret the velocity gradient $v_1 - v_2$ by a slip velocity v_g:

$$v_g = v_1 - v_2 = \frac{b}{2\eta} fL. \tag{57}$$

The final expression of the flow in each liquid is:

$$\begin{cases} v_1 &= \frac{f_1}{2\eta_1} \left(\left(\frac{L_1}{2} \right)^2 - z^2 \right) + \bar{v} + \left(1 + \frac{L_2\rho_2 - L_1\rho_1}{\rho_1 L_1 + \rho_2 L_2} \right) \frac{v_g}{2} \\ v_2 &= -\frac{f_2}{2\eta_2} \left(\left(\frac{L_2}{2} \right)^2 - z^2 \right) + \bar{v} - \left(1 + \frac{L_1\rho_1 - L_2\rho_2}{\rho_1 L_1 + \rho_2 L_2} \right) \frac{v_g}{2} \end{cases} \tag{58}$$

With:

$$\bar{v} = \left(\frac{\rho_2 L_2^2}{12\eta_2} - \frac{\rho_1 L_1^2}{12\eta_1} \right) \frac{fL}{\rho_1 L_1 + \rho_2 L_2}. \tag{59}$$

We thus have two Poiseuille flows in opposite directions and a global term which depends on the reference frame.

Linearity and slip lengths obtained

Liquid flow in a solid nanochannel

Fig. 8 represents the force-linearised velocity profiles obtained for both heptane and water flowing through channels of 8 nm and 12 nm for the four forces considered in each case. We can see that the response of the system is linear and that the velocity of the particles in the liquid is proportional to the force we applied on them. We can also see that the flows in heptane and water are in opposite directions. This intended for consistency with the liquid-liquid configuration.

Fig. 9 represents the force-linearised velocity profiles obtained for both heptane and water flowing through channels of 8 nm for the forces F_4 to F_2. The hydrodynamic prediction is also represented. As all profiles overlap, there is no significant changes in viscosity. The viscosity in the liquid is therefore close to that of the bulk.

The values of slip lengths of heptane on frozen water $b^{\mathrm{S}}_{\mathrm{h/w}}$ and of water on frozen heptane $b^{\mathrm{S}}_{\mathrm{w/h}}$ obtained in each case are reported in Table 5. The values of the forces are listed in Table 3 and Table 2. We can see that for both water and heptane, the slip lengths are of the order of a few angströms. That means that both liquids barely slip on the solid channel.

Table 5: Slip length of liquid heptane on frozen water $b^{\mathrm{S}}_{\mathrm{h/w}}$ and of water on frozen heptane $b^{\mathrm{S}}_{\mathrm{w/h}}$ obtained for different forces and channel widths. Av. : Average.

Channel	8 nm			12 nm			
Force	F_4	F_3	F_2	F_4	F_3	F_2	Av.
$b^{\mathrm{S}}_{\mathrm{h/w}}$ (nm)	0.22	0.10	0.18	0.13	0.11	0.08	0.136 ± 0.05
$b^{\mathrm{S}}_{\mathrm{w/h}}$ (nm)	0.24	0.13	0.19	0.13	0.17	0.19	0.175 ± 0.04

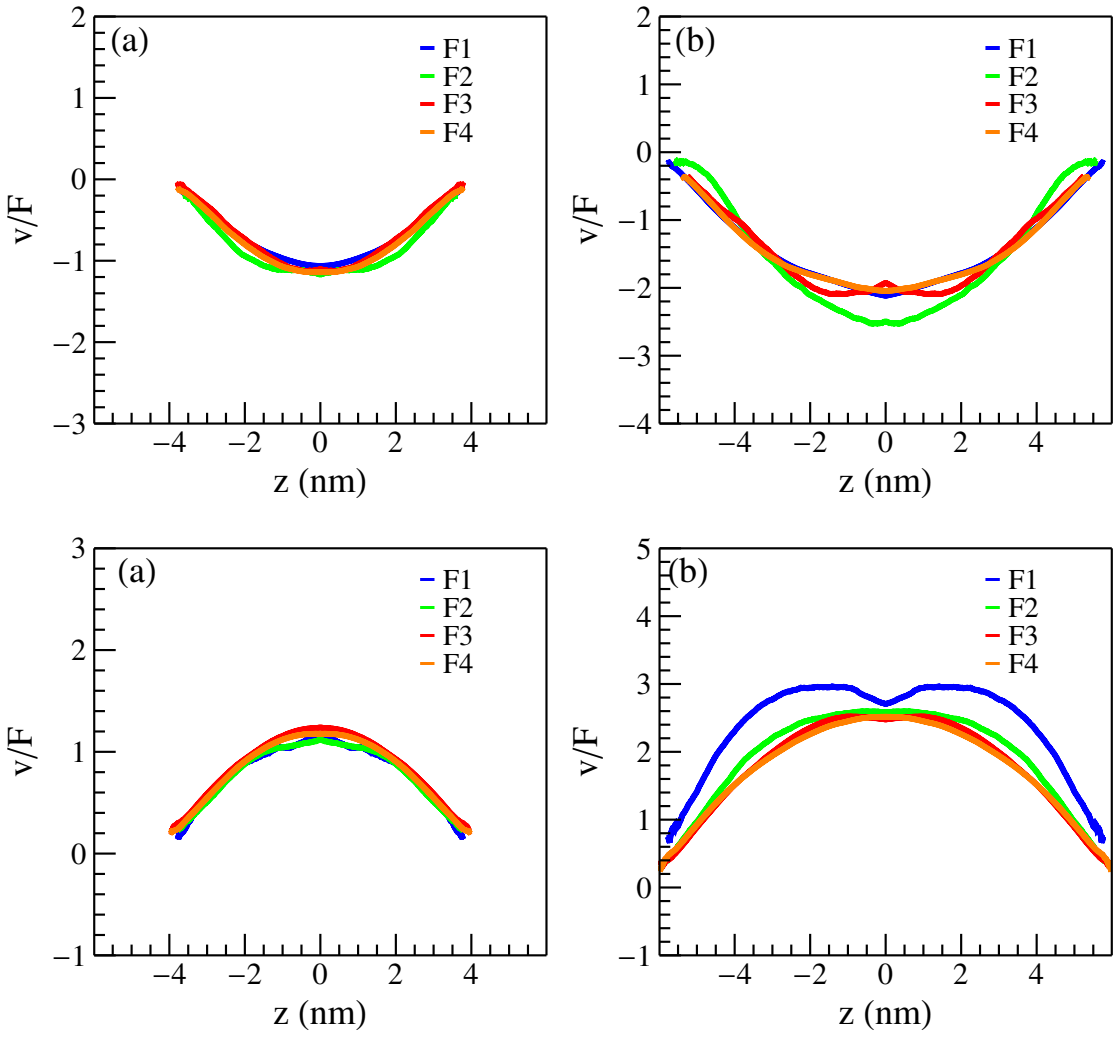

Figure 8: Force-linearised velocity profiles obtained for: (top) heptane flowing through a frozen water channel of witdh (a) 8 nm and (b) 12 nm, and (bottom) water flowing through a channel of (a) 8 nm and (b) 12 nm.

Two phase flow with liquid-liquid planar interface

Fig. 10 represents the force-linearised velocity profiles for the 8 nm/8 nm configuration and the 12 nm/12 nm configuration for the four forces considered in each case. We can see that the velocity of the particles in the liquid are proportional to the force applied on them in both liquid and in each configuration. The response of the system is therefore linear in the range of forces considered.

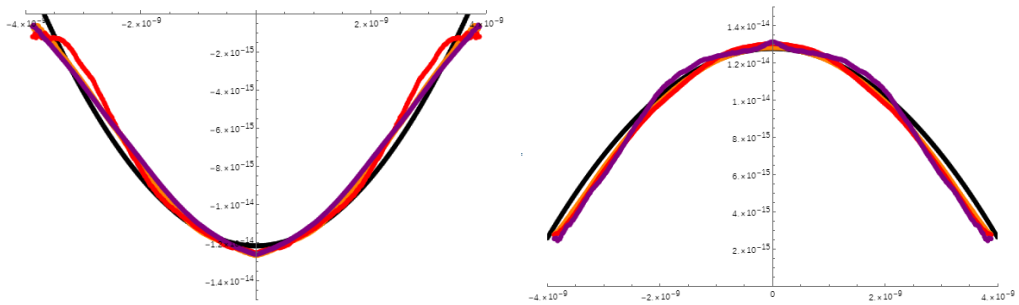

Figure 9: Force-linearised velocity profiles obtained for (left) heptane flowing through a frozen water channel of 8 nm and (right) water flowing through 8 nm for F_4 (orange), F_3 (red) and F_2 (purple) and hydrodynamics prediction (black).

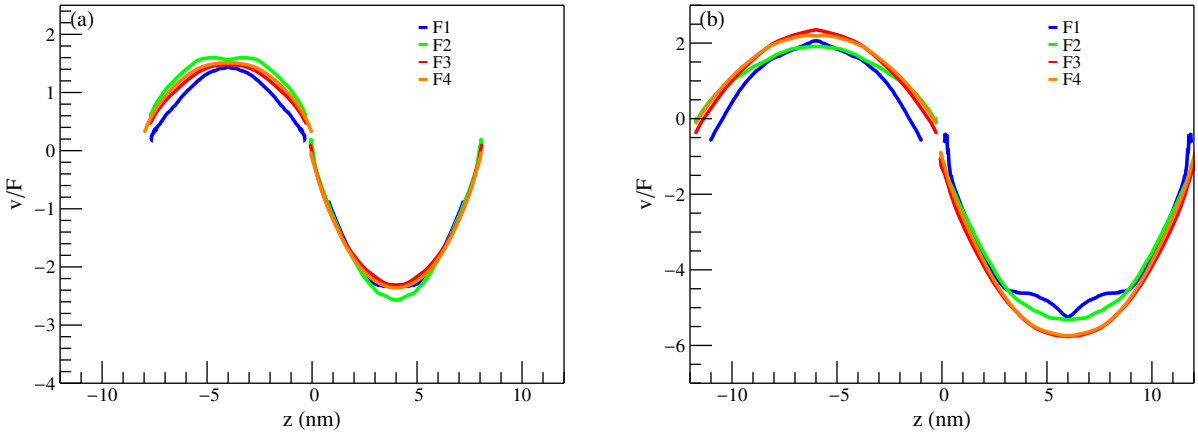

Figure 10: Force-linearised profiles obtained for the 8 nm/8 nm configuration (a) and the 12 nm/12 nm configuration (b).

Velocity and density profiles

This section provides the velocity and density profiles obtained in each case considered.

References

(1) Ellis, J. S.; Thompson, M. Slip and coupling phenomena at the liquid-solid interface. *PCCP* **2004**, *6*, 4928–4938.

(2) Quirke, N. *Adsorption and Transport at the Nanoscale*; 2006.

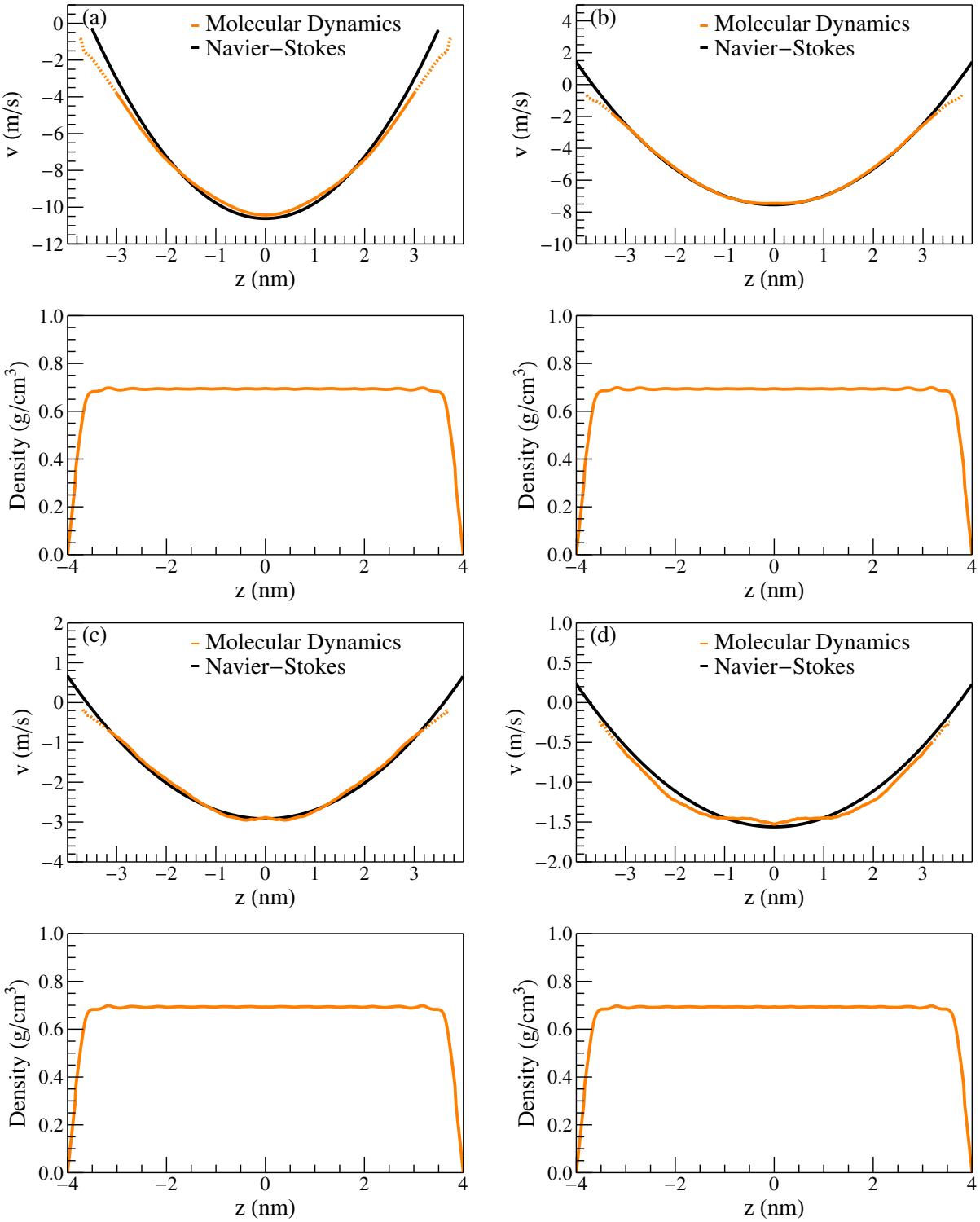

Figure 11: Velocity and density profiles obtained from MDS (in orange) and velocity fitted from Navier-Stokes equation (in black) for systems with heptane layer of 8 nm for the forces F_4 (a), F_3 (b), F_2 (c) and F_1 (d) given in Table 2.

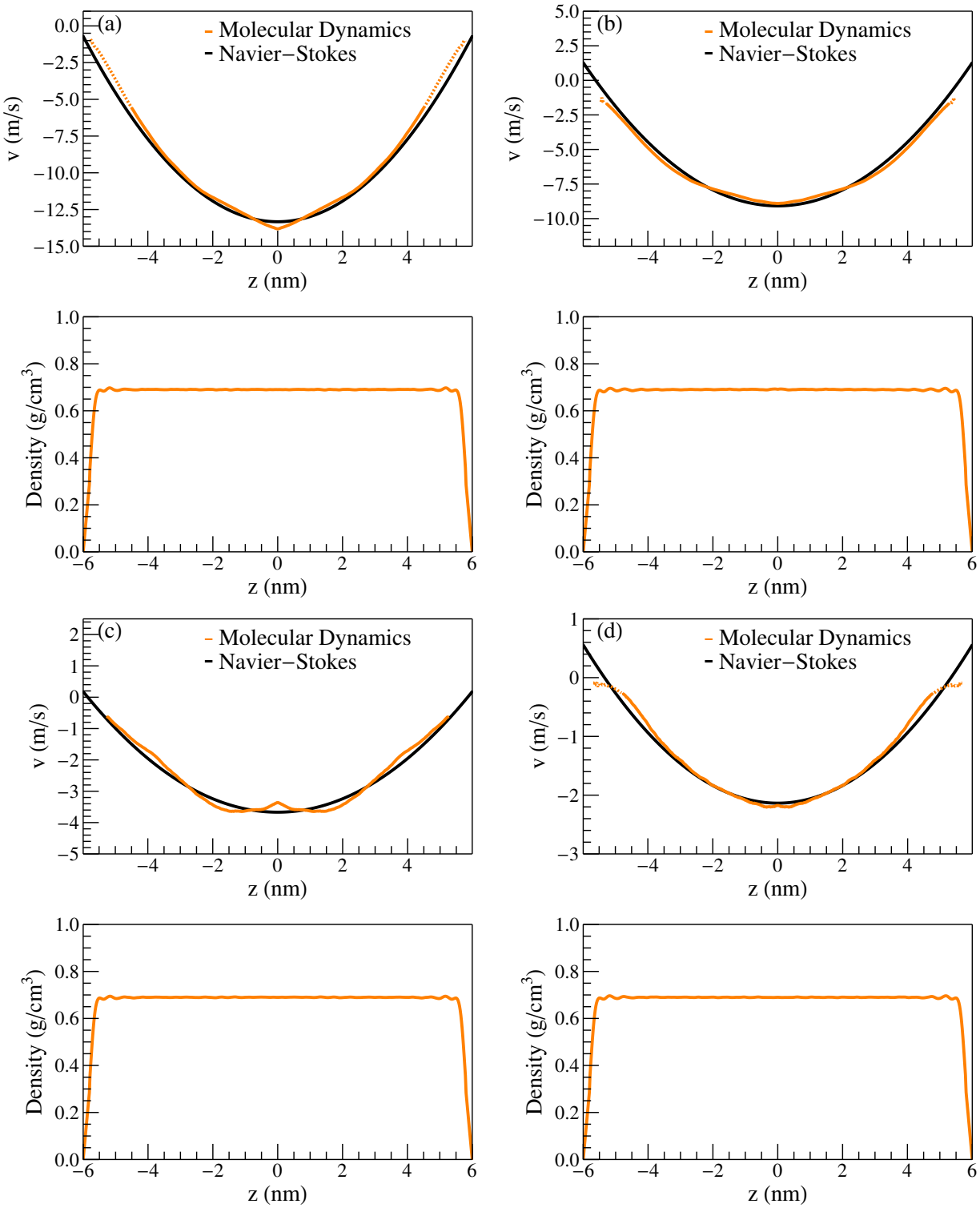

Figure 12: Velocity and density profiles obtained from MDS (in orange) and velocity fitted from Navier-Stokes equation (in black) for systems with heptane layer of 12 nm for the forces F_4 (a), F_3 (b), F_2 (c) and F_1 (d) given in Table 2.

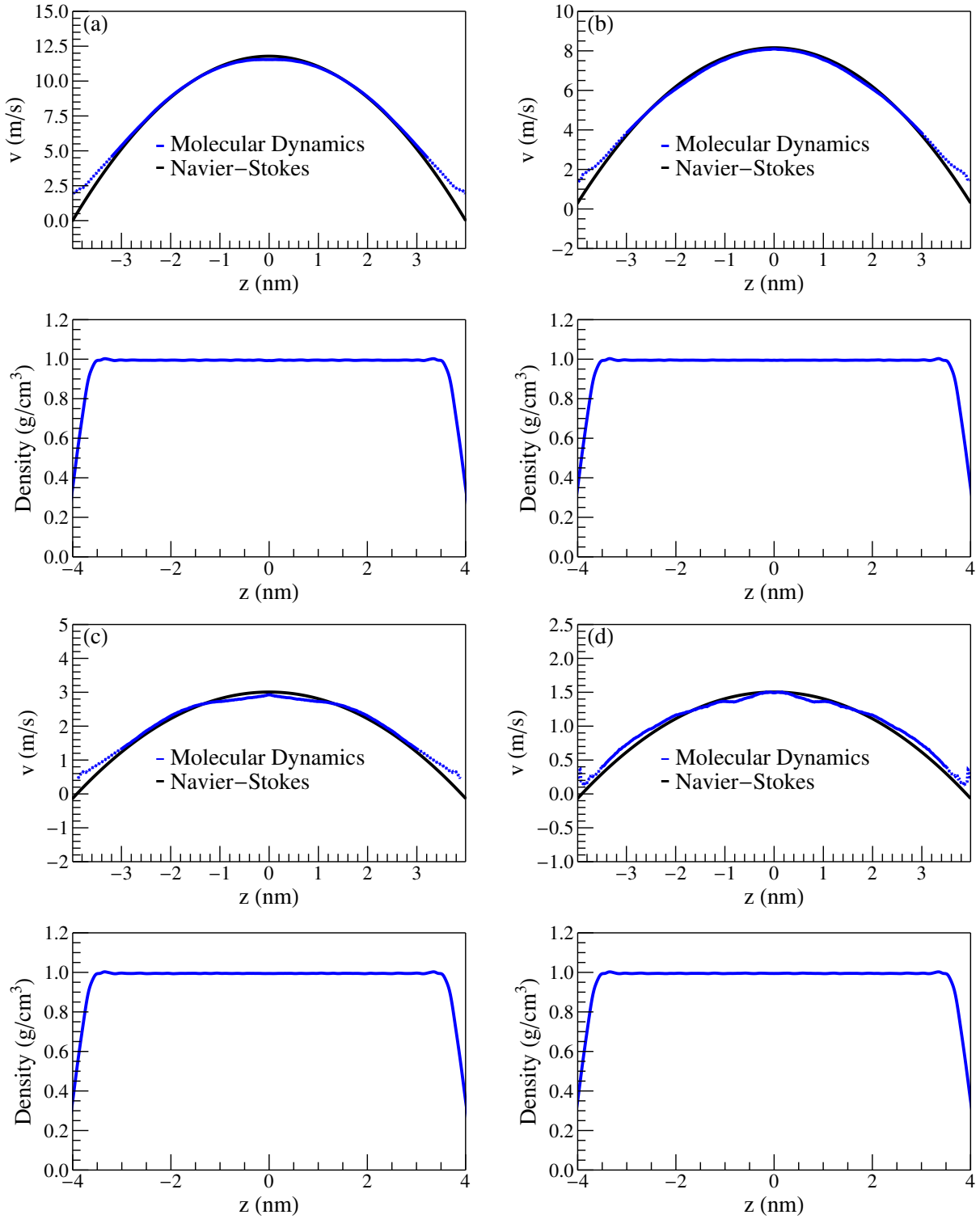

Figure 13: Velocity and density profiles obtained from MDS (in blue) and velocity fitted from Navier-Stokes equation (in black) for systems with water layer of 8 nm for the forces F_4 (a), F_3 (b), F_2 (c) and F_1 (d) given in Table 3.

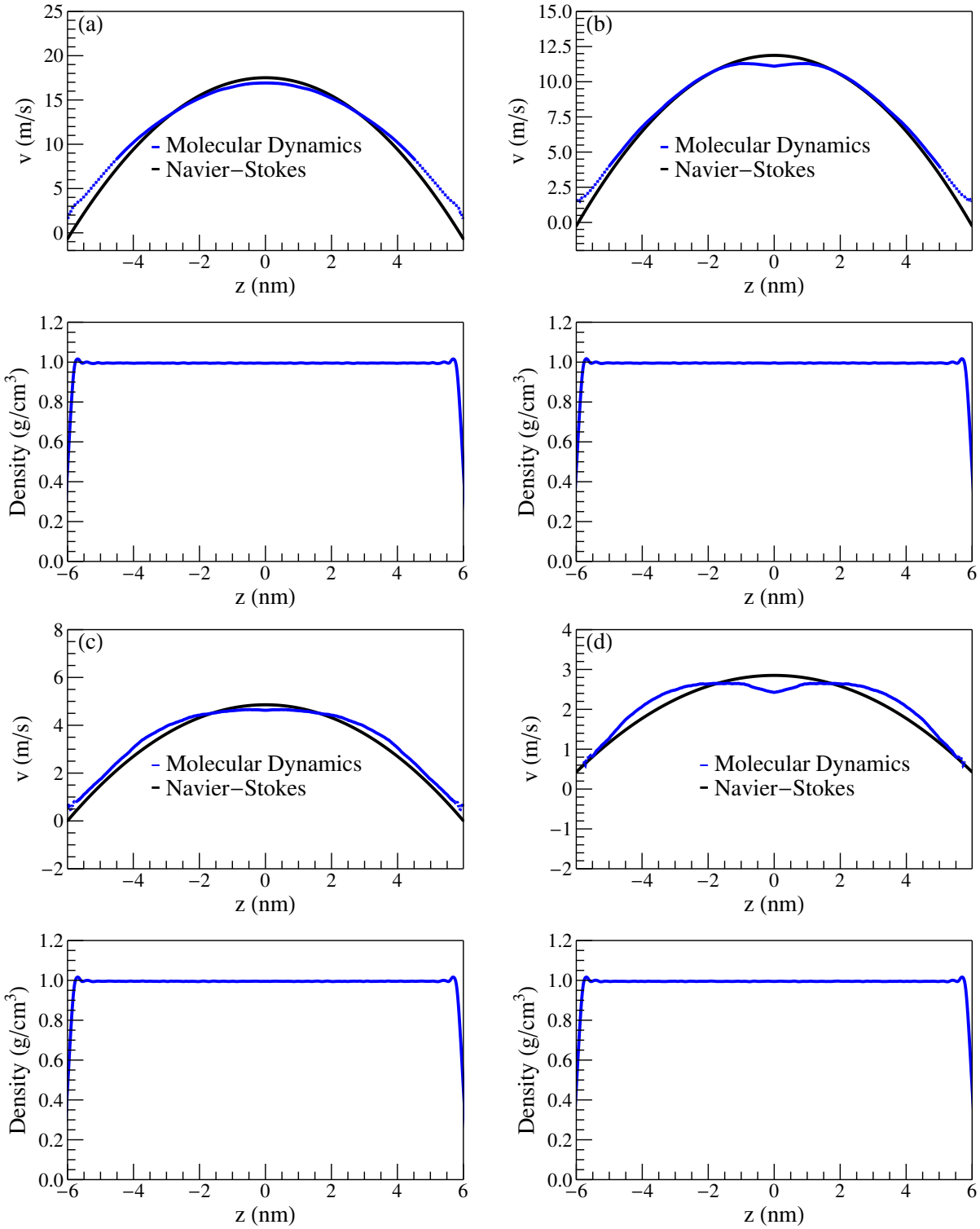

Figure 14: Velocity and density profiles obtained from MDS (in blue) and velocity fitted from Navier-Stokes equation (in black) for systems with water layer of 12 nm for the forces F_4 (a), F_3 (b), F_2 (c) and F_1 (d) given in Table 3.

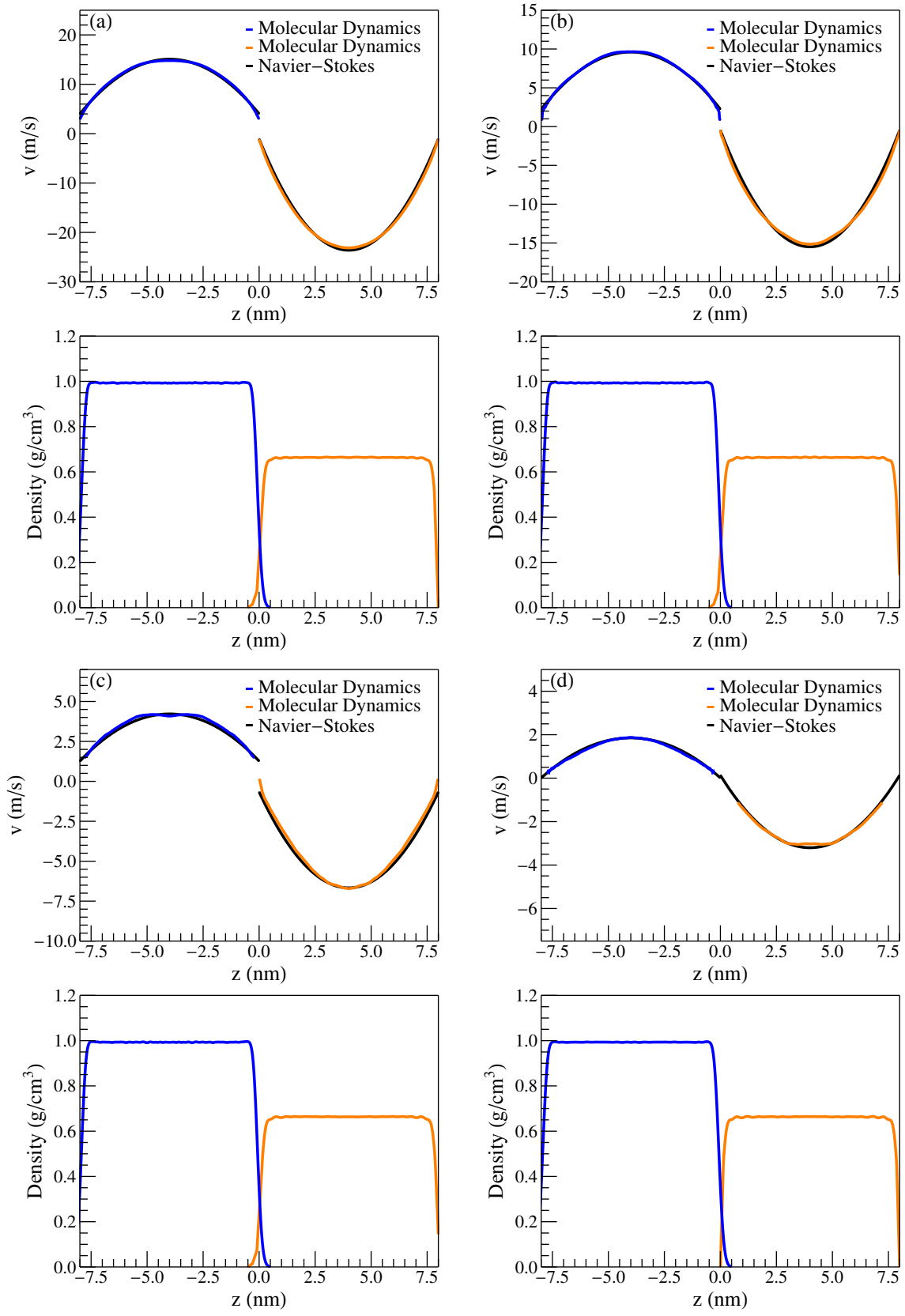

Figure 15: Velocity and density profiles obtained from MDS heptane (in orange) and for water (in blue) and velocity fitted from Navier-Stokes equations (in black) for a system with layers of 8 nm for forces F_4 (a), F_3 (b), F_2 (c) and F_1 (d) given in Table **??**.

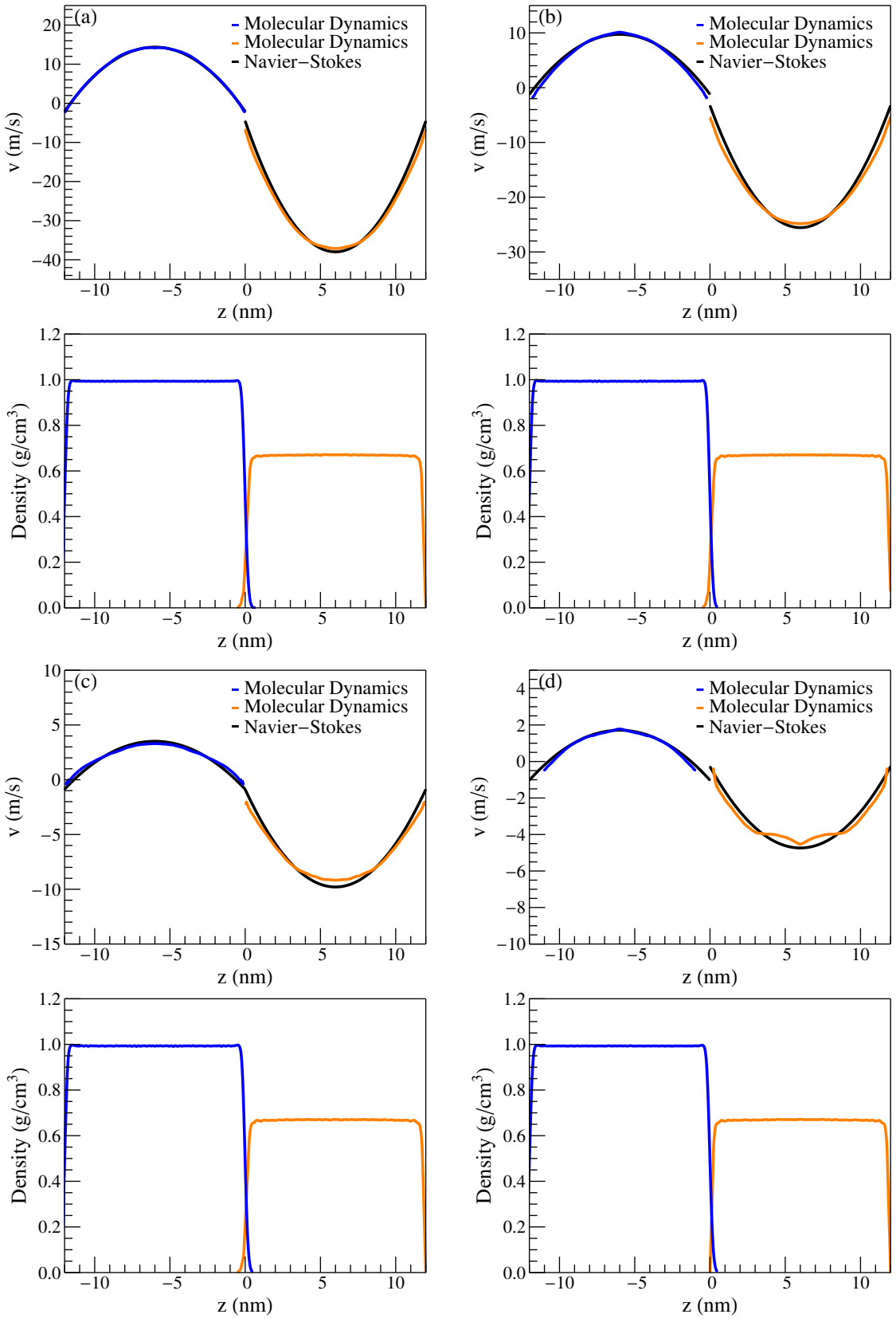

Figure 16: Velocity and density profiles obtained from MDS heptane (in orange) and for water (in blue) and velocity fitted from Navier-Stokes equations (in black) for a system with layers of 12 nm for forces F_4 (a), F_3 (b), F_2 (c) and F_1 (d). given in Table **??**.

(3) Patashinski, A. Z.; Ratner, M. A.; Orlik, R.; Mitus, A. C. Nanofluidic Manifestations of Structure in Liquids: A Toy Model. *J. Phys. Chem. C* **2019**, *123*, 16787–16795.

(4) Duan, C.; Zhou, F.; Jiang, K.; Yu, T. Molecular dynamics simulation of planar Poiseuille flow for polymer melts in atomically flat nanoscale channel. *Int. J. Heat Mass Transf.* **2015**, *91*, 1088–1100.

(5) Karniadakis, G. E.; Beskok, A.; Aluru, N. R. *Microflows and Nanoflows Fundamentals and Simulation*; 2005.

(6) Todd, B. D.; Daivis, P. J. Homogeneous non-equilibrium molecular dynamics simulations of viscous flow: Techniques and applications. *Mol. Simul.* **2007**, *33*, 189–229.

(7) Travis, K. P.; Todd, B. D.; Evans, D. J. Departure from Navier-Stokes hydrodynamics in confined liquids. *Phys. Rev. E* **1997**, *55*, 4288–4295.

(8) Di Leo, J. M.; Marañón, J. Water flow through nanopore. *Int. J. Quantum Chem.* **2008**, *108*, 1623–1628.

(9) Botan, A.; Rotenberg, B.; Marry, V.; Turq, P.; Noetinger, B. Hydrodynamics in Clay Nanopores. *J. Phys. Chem. C* **2011**, *115*, 16109–16115.

(10) Marry, V.; Rotenberg, B.; Turq, P. Structure and dynamics of water at a clay surface from molecular dynamics simulation. *PCCP* **2008**, *10*, 4802–4813.

(11) Sparreboom, W.; Van Den Berg, A.; Eijkel, J. C. Principles and applications of nanofluidic transport. *Nat. Nanotechnol* **2009**, 713–720.

(12) Bocquet, L.; Barrat, J. L. Hydrodynamic boundary conditions and correlation functions of confined fluids. *Phys. Rev. Lett.* **1993**, *70*, 2726–2729.

(13) Barrat, J. L.; Bocquet, L. Influence of wetting properties on hydrodynamic boundary conditions at a fluid/solid interface. *Faraday Discuss.* **1999**, *112*, 119–127.

(14) Bocquet, L.; Barrat, J. L. Flow boundary conditions from nano- to micro-scales. *Soft Matter* **2007**, *3*, 685–693.

(15) Dufreche, J. F.; Marry, V.; Malíková, N.; Turq, P. Molecular hydrodynamics for electro-osmosis in clays: From Kubo to Smoluchowski. *J. Mol. Liq.* **2005**, *118*, 145–153.

(16) Marry, V.; Dufrêche, J.-F.; Jardat, M.; Turq, P. Equilibrium and electrokinetic phenomena in charged porous media from microscopic and mesoscopic models: electro-osmosis in montmorillonite. *Mol. Phys.* **2003**, *101*, 3111–3119.

(17) Kumar Kannam, S.; Todd, B. D.; Hansen, J. S.; Daivis, P. J. Slip length of water on graphene: Limitations of non-equilibrium molecular dynamics simulations. *J. Chem. Phys.* **2012**, *136*, 024705.

(18) Ehlinger, Q.; Joly, L.; Pierre-Louis, O. Giant slip at liquid-liquid interfaces using hydrophobic ball bearings. *Phys. Rev. Lett.* **2013**, *110*, 1–5.

(19) Herrero, C.; Tocci, G.; Merabia, S.; Joly, L. Fast increase of nanofluidic slip in supercooled water: The key role of dynamics. *Nanoscale* **2020**, *12*, 20396–20403.

(20) Kuon, N.; Milischuk, A. A.; Ladanyi, B. M.; Flenner, E. Self-intermediate scattering function analysis of supercooled water confined in hydrophilic silica nanopores. *J. Chem. Phys* **2017**, *146*, 214501.

(21) Sendner, C.; Horinek, D.; Bocquet, L.; Netz, R. R. Interfacial water at hydrophobic and hydrophilic surfaces: Slip, viscosity, and diffusion. *Langmuir* **2009**, *25*, 10768–10781.

(22) Joly, L.; Ybert, C.; Trizac, E.; Bocquet, L. Liquid friction on charged surfaces: From hydrodynamic slippage to electrokinetics. *J. Chem. Phys* **2006**, *125*, 20476.

(23) Xie, Y.; Fu, L.; Niehaus, T.; Joly, L. Liquid-Solid Slip on Charged Walls: The Dramatic Impact of Charge Distribution. *Phys. Rev. Lett* **2020**, *125*, 1–7.

(24) Huang, D. M.; Sendner, C.; Horinek, D.; Netz, R. R.; Bocquet, L. Water Slippage versus Contact Angle: A Quasiuniversal Relationship. *Phys. Rev. Lett.* **2008**, *101*, 226101.

(25) Lang, S. B.; Wilke, C. R. A Hydrodynamic Mechanism for the Coalescence of Liquid Drops. I. Theory of Coalescence at a Planar Interface. *Ind. Eng. Chem. Fundam* **1971**, *10*, 22.

(26) Lang, S. B.; Wilke, C. R. A Hydrodynamic Mechanism for the Coalescence of Liquid Drops. II. Experimental Studies. *Ind. Eng. Chem. Fundam* **1971**, *10*, 341.

(27) Chesters, A. K. Modelling of coalescence processes in fluid-liquid dispersions. A review of current understanding. *Chem. Eng. Res. Des.* **1991**, *69*, 259–227.

(28) Eggers, J.; Lister, J. R.; Stone, H. A. Coalescence of liquid drops. *J. Fluid Mech.* **1999**, *401*, 293–310.

(29) Kovalchuk, K.; Riccardi, E.; Grimes, B. A. Multiscale modeling of mass transfer and adsorption in liquid-liquid dispersions. 1. Molecular dynamics simulations and interfacial tension prediction for a mixed monolayer of mono- and tetracarboxylic acids. *Ind. Eng. Chem. Res.* **2014**, *53*, 11691–11703.

(30) Lam, Y. C.; Jiang, L.; Li, L.; Yue, C. Y.; Tam, K. C.; Hu, X. Interfacial Slip at the Thermotropic Liquid-Crystalline Polymer/Poly (Ethylene Naphthalate) Interface. *J. Polym. Sci., Polym. Phys.* **2004**, *42*, 302–315.

(31) Barsky, S.; Robbins, M. O. Molecular dynamics study of slip at the interface between immiscible polymers. *Phys. Rev. E* **2001**, *63*, 0218011–0218017.

(32) Padilla, P.; Toxvaerd, S. Shear flow at liquid – liquid interfaces. *J. Chem. Phys* **1995**, *103*, 716–724.

(33) Koplik, J.; Banavar, J. R. Slip, immiscibility, and boundary conditions at the liquid-liquid interface. *Phys. Rev. Lett.* **2006**, *96*, 2–5.

(34) Galliero, G. Lennard-Jones fluid-fluid interfaces under shear. *Phys. Rev. E* **2010**, *81*, 1–7.

(35) Poesio, P.; Damone, A.; Matar, O. K. A multiscale approach to interpret and predict the apparent slip velocity at liquid-liquid interfaces. *J. Phys. Conf. Ser.* **2017**, *923*, 012003.

(36) Poesio, P.; Damone, A.; Matar, O. K. Slip at liquid-liquid interfaces. *Phys. Rev. Fluids* **2017**, *2*, 1–9.

(37) Zhan, S.; Su, Y.; Jin, Z.; Zhang, M.; Wang, W.; Hao, Y.; Li, L. Study of liquid-liquid two-phase flow in hydrophilic nanochannels by molecular simulations and theoretical modeling. *J. Chem. Eng.* **2020**, *395*, 125053.

(38) Herrero, C.; Omori, T.; Yamaguchi, Y.; Joly, L. Shear force measurement of the hydrodynamic wall position in molecular dynamics. *J. Chem. Phys.* **2019**, *151*.

(39) Omori, T.; Inoue, N.; Joly, L.; Merabia, S.; Yamaguchi, Y. Full characterization of the hydrodynamic boundary condition at the atomic scale using an oscillating channel: Identification of the viscoelastic interfacial friction and the hydrodynamic boundary position. *Phys. Rev. Fluids* **2019**, *4*, 114201.

(40) Oga, H.; Omori, T.; Herrero, C.; Merabia, S.; Joly, L.; Yamaguchi, Y. Theoretical framework for the atomistic modeling of frequency-dependent liquid-solid friction. *Phys. Rev. Res.* **2021**, *3*, 1–6.

(41) Jorgensen, W. L.; Maxwell, D. S.; Tirado-Rives, J. Development and Testing of the OPLS All-Atom Force Field on Conformational Energetics and Properties of Organic Liquids. *J. Am. Chem. Soc* **1996**, *118*, 11225–11236.

(42) Jorgensen, W. L.; Maxwell, D. S.; Tirado-Rives, J. Supporting Information: Developing and Testing of the OPLS All-Ato Force Field. 1996.

(43) Berendsen, H. J. C. The Missing Term in Effective Pair Potentials. *J. Phys. Chem* **1987**, *91*, 6269–6271.

(44) Eastwood, J.; Hockney, R.; Lawrence, D. P3M3DP The three-dimensional periodic particle-particle/ particle-mesh program. *Comput. Phys. Commun* **1980**, *19*, 215–261.

(45) Ryckaert, J.-P.; Ciccotti, G.; Berendsen, H. J. C. Numerical integration of the Cartesian Equations of Motion of a System with Constraints: Molecular Dynamics of n-Alkanes. *J. Comput. Phys.* **1977**, *23*, 321–341.

(46) Vatin, M.; Duvail, M.; Guilbaud, P.; Dufrêche, J. F. Liquid/liquid interface in periodic boundary condition. *PCCP* **2021**, *23*, 1178–1187.

(47) Plimpton, S. Fast Parallel Algorithms for Short-Range Molecular Dynamics. *J. Comput. Phys.* **1995**, *117*, 1–19.

(48) Frenkel, D.; Smit, B. In *Understanding Molecular Simulations*, 2nd ed.; Academic Press,, Ed.; 2009; p 628.

(49) Bernardi, S.; Todd, B. D.; Searles, D. J. Thermostating highly confined fluids. *J. Chem. Phys.* **2010**, *132*.

(50) Sam, A.; Kannam, S. K.; Hartkamp, R.; Sathian, S. P. Water flow in carbon nanotubes: The effect of tube flexibility and thermostat. *J. Chem. Phys.* **2017**, *146*.

(51) Sega, M.; Jedlovszky, P. The impact of tensorial temperature on equilibrium thermodynamics. *PCCP* **2018**, *20*, 16910–16912.

(52) Kubo, R. Statistical-Mechanical Theory of Irreversible Processes. I. General Theory and Simple Applications to Magnetic and Conduction Problems. *J. Phys. Soc. of Japan* **1957**, *12*, 570–586.

(53) Green, M. S. Markoff random processes and the statistical mechanics of time-dependent phenomena. II. Irreversible processes in fluids. *J. Chem. Phys.* **1954**, *22*, 398–413.

(54) Cui, S. T.; Cummings, P. T.; Cochran, H. D. The calculation of the viscosity from the autocorrelation function using molecular and atomic stress tensors. *Mol. Phys.* **1996**, *88*, 1657–1664.

(55) Tazi, S.; Boan, A.; Salanne, M.; Marry, V.; Turq, P.; Rotenberg, B. Diffusion coefficient and shear viscosity of rigid water models. *J. Condens. Matter Phys.* **2012**, *24*, 284117.

(56) González, M. A.; Abascal, J. L. The shear viscosity of rigid water models. *J. Chem. Phys.* **2010**, *132*, 096101.

(57) Mondello, M.; Grest, G. S. Viscosity calculations of n-alkanes by equilibrium molecular dynamics. *J. Chem. Phys.* **1997**, *106*, 9327–9336.

(58) Kondratyuk, N. *J. Chem. Phys.*

(59) Kouris, S.; Panaylotou, C. Dynamic Viscosity of Mixtures of Benzene, Ethanol, and n-Heptane at 298.15 K. *J. Chem. Eng. Data* **1989**, *34*, 200–203.

(60) Velásquez, A. M.; Hoyos, B. A. Viscosity of heptane-toluene mixtures. Comparison of molecular dynamics and group contribution methods. *J. Mol. Model.* **2017**, *23*, 1–9.

(61) Bocquet, L.; Barrat, J.-L. On the Green-Kubo relationship for the liquid-solid friction coefficient. *J. Chem. Phys.* **2013**, *139*, 44704.

(62) Varghese, S.; Hansen, J. S.; Todd, B. D. Improved methodology to compute the intrinsic friction coefficient at solid-liquid interfaces. *J. Chem. Phys* **2021**, *154*.

(63) Bocquet, L.; Charlaix, E. Nanofluidics, from bulk to interfaces. *Chem. Soc. Rev.* **2010**, *39*, 1073–1095.

(64) Falk, K.; Sedlmeier, F.; Joly, L.; Netz, R. R.; Bocquet, L. Ultralow liquid/solid friction in carbon nanotubes: Comprehensive theory for alcohols, alkanes, OMCTS, and water. *Langmuir* **2012**, *28*, 14261–14272.

(65) Smolyanitsky, A.; Kazakov, A. F.; Bruno, T. J.; Huber, M. L. Mass diffusion of organic fluids: a molecular dynamics perspective. *Natl. Inst. Stand. Technol. Tech. Note 1805* **2013**,

TOC Graphic